Global and Planetary Change 253 (2025) 104966

Contents lists available at ScienceDirect

Global and Planetary Change

journal homepage: www.elsevier.com/locate/gloplacha

Paleoredox, iron cycling, and primary productivity in the late Devonian of southern Laurussia (Woodford Shale, Oklahoma, USA)☆

Austin J. McGlannan [a], Jeremy D. Owens [b], Seth A. Young [b], Sean M. Newby [b,c], Derek Parks [a], Xiao-Lei Liu [a], Caitlin Hodges [a], Andrew Cullen [d], Gerilyn S. Soreghan [a,*]

[a] The University of Oklahoma, School of Geosciences, Norman, OK 73019, USA
[b] Florida State University, Department of Earth, Ocean, and Atmospheric Sciences, and National High Magnetic Field Laboratory, Tallahassee 32306, USA
[c] The University of Hong Kong, Department of Earth Sciences, Hong Kong, China
[d] Independent Geoscientist, Norman, OK 73072, USA

ARTICLE INFO

Editor: Dr. Maoyan Zhu

Keywords:
Black shale
Bioavailable iron
Iron shuttle
Dust

ABSTRACT

Upper Devonian mudstones that accumulated in southern Laurussian epeiric seas, and correlatives across Laurussia sequestered globally significant volumes of organic carbon, recording high biological productivity and, potentially, anoxic conditions. However, factors driving productivity and carbon cycling in this system remain poorly constrained. Here we present geochemical data on total organic carbon, iron speciation, molybdenum and vanadium concentrations, and lipid biomarkers (C_{40} aromatic carotenoids, porphyrins, Methyltrimethyltridecylchroman, and α-tocopherol quinone) to provide insights on water column redox conditions, primary productivity, and mechanisms of delivery of highly reactive iron species to the Devonian Woodford Shale on the southern Laurussian continental shelf. These data demonstrate the operation of a dynamic chemocline across the shelf, with anoxic-sulfidic conditions generally prevailing through the lower and middle Woodford Shale, and anoxic to oxic conditions with intermittent euxinia prevailing during deposition of the upper Woodford Shale. Chemocline fluctuations in this region may reflect responses to global climate fluctuations near the Frasnian – Famennian and Famennian – Tournaisian boundary intervals–the latter associated with onset of the Late Paleozoic Ice Age. During times of extended euxinia, the Woodford Shale system acted as an iron sink, sequestering iron in the form of pyrite. In contrast, during intervals of more oxic and less-sulfidic conditions, particularly during deposition of the upper Woodford Shale, the shelf sourced iron that diffused from sediment porewaters into the overlying water column (the iron shuttle) and promoted biologic productivity. Additionally, allochthonous iron may have entered the system in the form of atmospheric dust and wildfire aerosols. Multiple sources of highly reactive iron in this system likely aided primary productivity and the carbon sequestration that occurred here and in many analogous and correlative units deposited in the lead-up to the Late Paleozoic Ice Age.

1. Introduction

The Late Devonian (Frasnian – Famennian) was a time of large paleoclimatic and paleoceanographic changes marked by global marine anoxia, mass extinctions, radiation and expansion of deep-rooted vascular land plants, and the initial onset of the Late Paleozoic Ice Age (LPIA) (Fig. 1; Joachimski et al., 2009; McGhee, 2013; Montañez and Poulsen, 2013; Zhang et al., 2021). This climatic shift is often ascribed to the expansion and radiation of land plants, which lowered atmospheric pCO_2 and increased pO_2 (Dahl and Arens, 2020). In addition to photosynthetic drawdown of atmospheric carbon by newly evolved widespread land plants, marine primary productivity and organic carbon preservation sequestered significant carbon in globally extensive epeiric seas in the form of black shales. The nutrient transport processes that fueled marine primary productivity are typically ascribed to 1) upwelling (Parrish, 1982; Turner and Slatt, 2016; Cardott and Comer, 2021) and 2) nutrient-rich terrigenous runoff attributable to the evolution and enhanced weathering effects of vascular land plants (Algeo et al., 1995; Algeo and Scheckler, 1998). The result was eutrophication of the marine shelves that fueled anoxia and euxinia (sulfidic water-

☆ This article is part of a Special issue entitled: 'Deep time Earth's climate' published in Global and Planetary Change.

* Corresponding author.
E-mail address: lsoreg@ou.edu (G.S. Soreghan).

https://doi.org/10.1016/j.gloplacha.2025.104966
Received 10 August 2024; Received in revised form 15 June 2025; Accepted 28 June 2025
Available online 1 July 2025

column conditions) which promoted the preservation of organic carbon in shallow marine strata globally (Algeo et al., 1995; Algeo and Scheckler, 1998; Algeo et al., 2001; Zhang et al., 2020). While the hypothesis of elevated nutrient flux from terrestrial runoff is widely recognized, the models for nutrient delivery, such as iron (Fe) cycling and the transport of bioavailable iron to distal marine environments, remain underexplored for the Devonian.

Iron is essential for all life. For primary producers, iron facilitates the transfer of electrons in the electron transport chain during photosynthesis and cellular respiration in addition to carrying out many other vital functions (Geider and La Roche, 1994). Thus, iron is a limiting nutrient that influences organic productivity and carbon cycling (Martin, 1990; Kolber et al., 1994; Martínez-García et al., 2014). Although iron is abundant in Earth's crust, the supply of (bioavailable; $Fe^{2+}_{(aq)}$) iron in oxic marine waters is limited owing to 1) its low solubility, and 2) suitable transfer mechanisms to the marine system—especially those distal from regions of continental runoff. The solubility of iron in seawater is controlled by numerous factors including oxidation state [Fe (II) vs Fe(III)], Fe mineralogy, particle size, photochemistry, atmospheric acidity, the concentration of organic ligands, seawater pH, and marine redox conditions such that iron is most soluble within anoxic to marginally sulfidic conditions (Kuma et al., 1996; Rickard, 2006; Rickard and Luther, 2007; Gledhill and Buck, 2012; Pohl and Fernández-Otero, 2012; Lv et al., 2022). Iron enters the marine system from river discharge, hydrothermal vents, iceberg melt, and delivery by eolian dust. Sedimentary benthic shuttling can further transfer iron in marine environments from shelfal environments to deep basins (Raiswell and Anderson, 2005).

The Fe transported into the marine system from terrigenous reservoirs exists in a range of mineral species comprising the total iron pool (Fe_T). Fe_T includes unreactive Fe (Fe_U), poorly reactive Fe (Fe_{PR}) such as silicate minerals, and highly reactive Fe (Fe_{HR}), where the term "highly reactive" refers to the reactivity of various Fe minerals that can be easily dissolved and reincorporated into other Fe phases (Poulton et al., 2004). The Fe_{HR} fraction encompasses Fe in (oxyhydr-)oxides (Fe_{ox}; ferrihydrite, lepidocrocite, goethite, hematite), Fe in magnetite (Fe_{mag}), Fe in carbonate minerals (Fe_{carb}; siderite, ankerite), and Fe in pyrite (Fe_{py}). Therefore, the Fe_{HR} fraction is the summation of Fe_{ox}, Fe_{carb}, Fe_{mag}, and Fe_{py} (Poulton and Canfield, 2005; Raiswell et al., 2018; Poulton, 2021). Since Fe_{HR} species are more soluble than Fe_{PR} and Fe_U, the Fe_{HR} fractions can become bioavailable ($Fe^{2+}_{(aq)}$) following physical, chemical and biological processing (Pohl and Fernández-Otero, 2012; Lv et al., 2022). Therefore, the Fe_{HR} fraction can serve as a proxy for bioavailable iron in ancient marine environments. These Fe_{HR} species are further enriched within anoxic marine environments wherein Fe_{HR} can additionally serve as a proxy for local paleoredox conditions.

In this contribution, we study the factors driving productivity and carbon cycling in the upper Devonian-lower Carboniferous Woodford Shale—a world-class source rock correlative to many black shales across North America and the globe. We investigate the paleoredox conditions to assess potential mechanisms for introducing bioavailable (Fe_{HR}) iron to this system, and, by integrating iron speciation data with trace metal and lipid biomarker data, we also test the hypothesis that highly reactive iron-bearing dust contributed to primary productivity. Results reveal the operation of a dynamic chemocline and provide new insights on the mechanisms surrounding Fe nutrient delivery in this and analogous systems and their potential influence on carbon cycling in the run-up to the LPIA.

2. Geological and geochemical background

2.1. Late Devonian paleoclimate, paleooceanography, paleogeography

While greenhouse conditions prevailed through much of the Late Devonian, episodes of global cooling began near the end of the Frasnian stage (Joachimski and Buggisch, 2002; Joachimski et al., 2009). Glaciation by the end Famennian is well accepted; however, the initiation for the timing of Gondwanan glaciation remains unresolved. Streel et al.

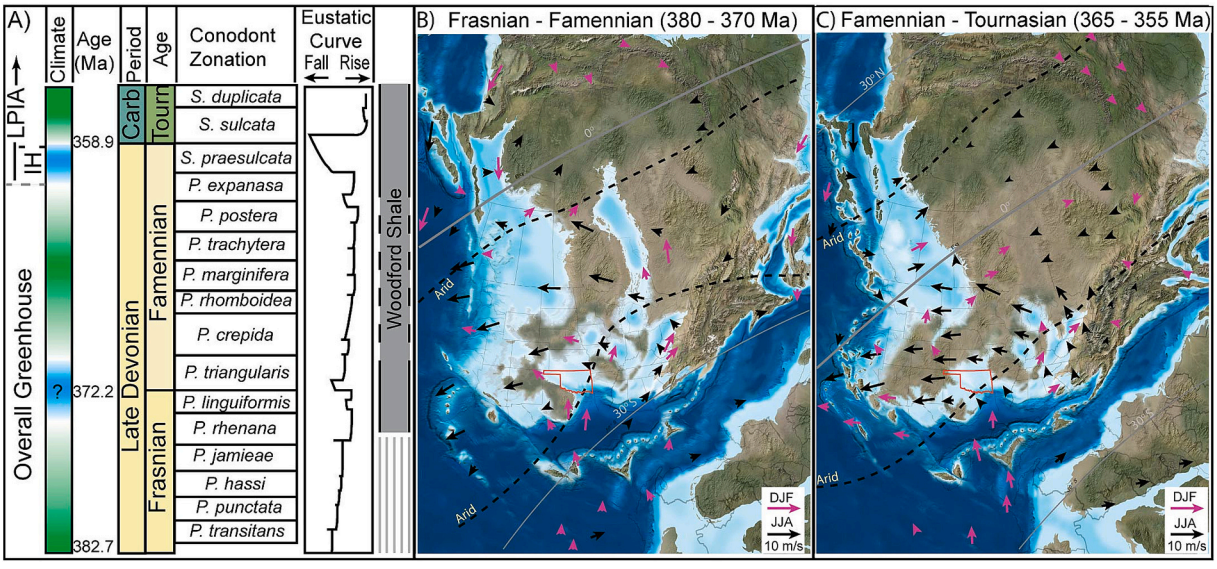

Fig. 1. Chronostratigraphy of the Woodford Shale and Late Devonian – early Mississippian paleogeographic reconstruction. A) Late Devonian–early Carboniferous Geological Time Scale displaying inferred greenhouse and icehouse climates. Eustatic sea-level curve adapted from Algeo et al. (2007). Woodford Shale chronostratigraphic time span is shown in grey. Solid borders represent known conodont biostratigraphic control of the Woodford Shale (Over, 1990), whereas the dashed boarders represent inferred depositional time frame. Geological timescale and age in Ma adapted from Cohen et al. (2013). Conodont genus abbreviations: *P.* – *Palmatolepis*; *S.* – *Siphonodella*. B) Paleogeographic map spanning the Frasnian – Famennian transition (380–370, ~375, Ma). C) Paleogeographic maps with seasonal wind circulations for the Famennian – Tournaisian transition (365–355, ~360 Ma). Black arrows are surface winds for months of December–January-February (DJF), purple arrows are surface winds for the months June–July-August (JJA). Paleogeographic maps are from Blakey (2013) North American Key Time Slices ©2013 Colorado Plateau Geosystems, Inc. Climate boundaries are from Boucot et al. (2013) and Scotese and Wright (2018). Surface wind models are adapted from the supplemental files in McGlannan et al. (2022). (For interpretation of the references to colour in this figure legend, the reader is referred to the web version of this article.)

(2000) reported cool and dry climate within the VH miospore zonation (middle to late *Palmatolepis gracilis expanasa* conodont zonation), with glaciation in the uppermost Famennian established in the LN – VI miospore zone (middle to late *Siphonodella praesulcata* conodont zonation). Lakin et al. (2016) provided a tighter constraint on glaciation with Gondwanan tillites recording an earliest date within the LE miospore zonation (early *Siphonodella praesulcata* conodont zonation). Isaacson et al. (2008) reported tills in Gondwana as early as the GF to VCo miospore zonation (late *Palmatolepis trachytera* to *Palmatolepis perlobata postera* conodont zonation). Climate cooling intensified through the latest Devonian, peaking in the late *Siphonodella praesulcata* zone (between the LE-LN miospore zones) with the occurrence of alpine glaciation in relatively low latitudes. Specific latitudes remain debated, with Brezinski et al. (2009, 2010) suggesting ~30 to ~35°S, while paleogeographic reconstructions in Blakey (2013) illustrate ~15° to 25°S (Fig. 1) in what is now the central Appalachians (Isaacson et al., 2008; Brezinski et al., 2008, 2009, 2010; Lakin et al., 2016).

Elevated marine primary productivity and global burial of organic carbon in black shales ensued during both greenhouse and icehouse intervals of the Late Devonian, leading to the development of an

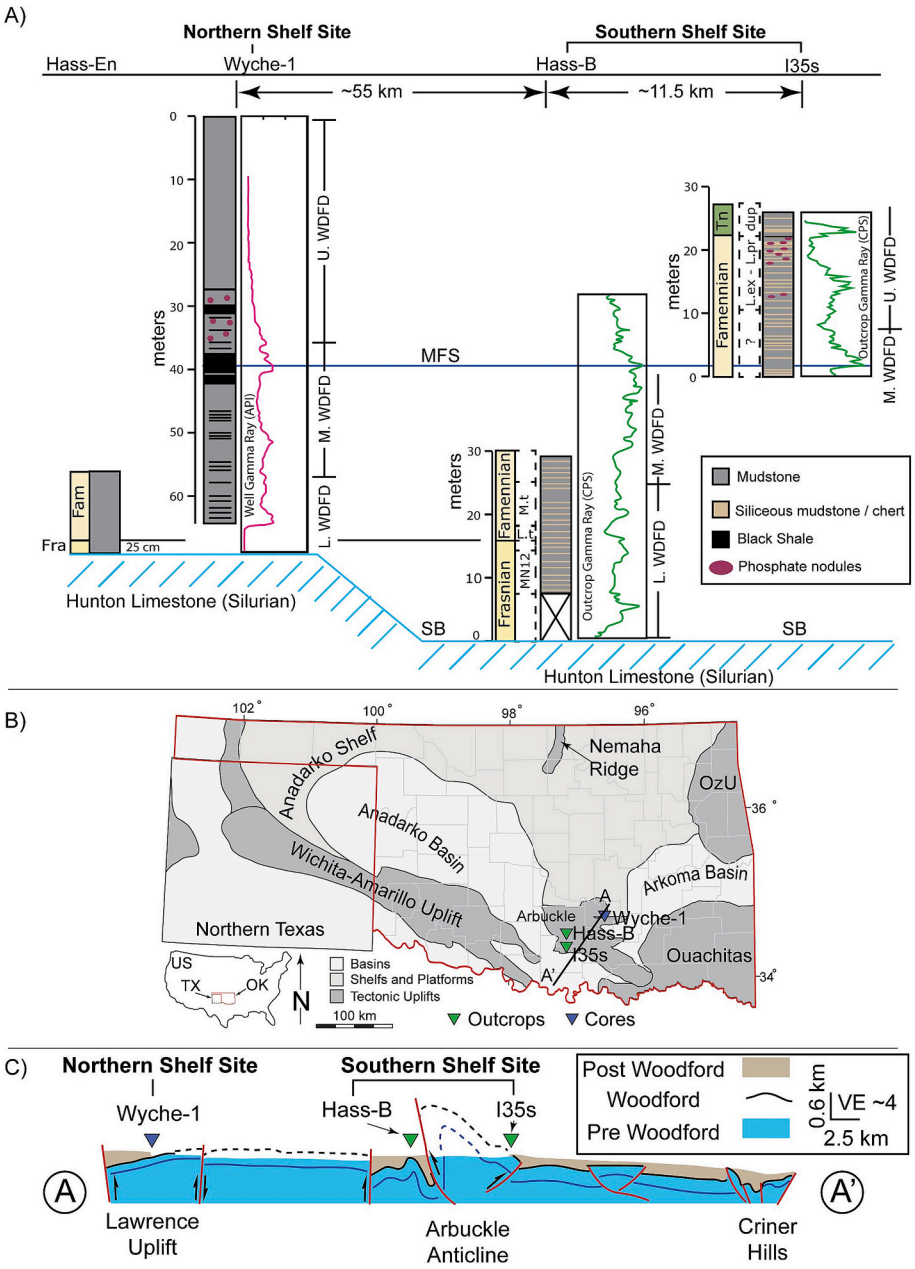

Fig. 2. Site location and chronostratigraphy of the Woodford Shale. A) Site chronostratigraphy and sequence stratigraphy of the Woodford Shale. Well gamma ray in API units for the northern shelf site, Wyche-1 core, is from Turner et al. (2015) and Molinares-Blanco (2019). Outcrop gamma ray in counts per second (CPS) for Hass-B and I35-south sections of the southern shelf site were derived from Aufill (2007) and Becerra et al. (2018) respectively. Conodont zonations of the sites are from Over, 1990 and Crick et al., 2002. The Hass-En site is illustrated to show the change in thickness between the northern shelf site on the Lawrence Uplift versus the southern shelf site in the Arbuckles. Details on Hass-En biostratigraphy are from Over, 1990. Conodont abbreviations are as follows: L.ex – late *expanasa,* L.pr – Late *praesulcata*, M.t – Middle *triangularis*. Fra – Frasnian, Fam – Famennian, Tn – Tournaisian. MFS – Maximum Flooding Surface, SB – Sequence Boundary. B) Site locations plotted on a tectonic map of Oklahoma. Map shows the current distribution of major basins and tectonic uplifts. Map modified from Campbell et al. (1988), Northcutt and Campbell (1995) and Miller et al. (2021). C) Northeast – southwest oriented cross section across major tectonic features of southern Oklahoma. Triangles note the location of study sites. Cross section adapted from Cullen and Hull, 2023.

estimated 8 % of global hydrocarbon source rocks (Ulmisheke and Klemme, 1990; Algeo and Scheckler, 1998; Dahl and Arens, 2020). For example, organic-rich Frasnian to lower Famennian black shales account for 10 % of North Africa's generated hydrocarbons (Lüning et al., 2003). Frasnian and Famennian black shales within South American basins include the Jandiatuba Formation (Solimoes Basin), Barreirinha Formation (Amazonas Basin), and Los Manos and Iquiri Formations (Chaco Basin; Loboziak et al., 1996; Milani and Zalán, 1999). By the onset of the late Famennian glaciation, many of these stratigraphic sections in South America include glaciomarine strata, fluvio-deltaic deposits and unconformities. In contrast, across Laurussia, correlative black shales accumulated across an expansive epeiric sea (~3000 km) between the Acadian orogen on the eastern margin and the Antler orogen in the west. These include the Chattanooga Shale (Appalachian Basin), New Albany Shale (Illinois Basin), Woodford Shale (southern Laurussia continental margin), Bakken Shale (Williston Basin), Exshaw Formation (Western Canadian Basin), and Duvernay Shale (Western Canadian Basin).

2.2. Woodford Shale geological overview

The Woodford Shale is an organic-rich siliceous marine mudstone deposited on a broad epicontinental shelf along the southern Laurussian margin. The unit includes upwards of 17 % total organic carbon (TOC) type II oil-prone kerogen (Comer, 1992; Romero and Philp, 2012; Connock et al., 2018). Additional components include detrital silt, siliceous tests of radiolaria and *Tasmanites,* illitic clay, and minor dolomite that accumulated in open-marine conditions far-removed from land and far from any fluvio-deltaic feeder systems (Kirkland et al., 1992; Turner et al., 2015; Kondas et al., 2018; Cardott and Comer, 2021; McGlannan et al., 2022). McGlannan et al. (2022) interpreted the detrital siliciclastic silt in the Woodford Shale to have originated in and deflated from Acadian clastic wedges (e.g. the Catskill Delta), and undergone wind transport and ultimate deposition into marine environments of the southern continental margin (Fig. 1). Deflation from subaerially desiccated Gondwanan depositional systems is also possible, although this hypothesis requires further testing.

The Woodford Shale is commonly divided into informal lower, middle, and upper subdivisions (Fig. 2; Cardott and Comer, 2021). The lower Woodford Shale locally includes a basal glauconitic green shale superseded by predominantly argillaceous mudstone and siliceous mudstone. The lower Woodford Shale developed under predominantly anoxic conditions with episodic pulses of photic-zone euxinia (PZE) (Connock et al., 2018; Parks and Liu, 2023). The middle Woodford Shale comprises massive to laminated siliceous mudstone and black siliceous mudstone with locally common framboidal and nodular pyrite (Figs. 3, 4; Turner et al., 2015; Galvis et al., 2018; Connock et al., 2018). Elevated values of C_{40} aromatic carotenoids and gammacerane indicate that the middle Woodford Shale experienced a sustained, strongly stratified water column with persistent PZE (Fig. 5; Connock et al., 2018; Philp and DeGarmo, 2020; Parks and Liu, 2023). The upper Woodford Shale in southern Oklahoma comprises highly siliceous and laminated argillaceous mudstone with widely occurring phosphate nodules and chert interbeds resulting from intensified radiolarian blooms (Figs. 3, 4). While biostratigraphic studies document the presence of some minor intraformational disconformities (Over, 1990, 1992; Over and Barrick, 1990; Schwartzapfel and Holdsworth, 1996; Crick et al., 2002; Kondas et al., 2018), studies using gamma-ray, lithology, geochemistry and biostratigraphic data suggest the lower through basal upper Woodford Shale is an overall transgressive system, with most of the upper Woodford Shale recording regression, although the lithologic indicators of this shift are minimal (Fig. 2; Slatt and Rodriguez, 2012; Turner et al., 2015, 2016; Kondas et al., 2018).

Although biostratigraphic ages within the Woodford Shale are challenging owing to sparse biota and poor microfossil preservation, analyses of conodonts, radiolarians, and palynomorphs show that the Woodford Shale spans Late Devonian – Early Carboniferous time, Figs. 1, 2). Conodont biostratigraphy, in some cases integrated with magnetostratigraphy (Crick et al., 2002), enables the placement of the Frasnian – Famennian and the Devono-Carboniferous boundaries in several localities. Conodont zonations establish that Woodford Shale deposition began in the lower *Palmatolepis rhenana* (Late Frasnian) and ended within the Early Tournaisian (Mississippian) upper *Siphonodella duplicata* conodont zones (Over, 1990; Fig. 2). Conodont biostratigraphy consistently places the Frasnian-Famennian boundary within the lower Woodford Shale approximately 0.2–16 m above the Silurian Hunton Limestone unconformity (Over, 1990; Fig. 3). Regional biostratigraphic correlations show that both the Frasnian and Famennian sections

Fig. 3. Lower, middle, and upper Woodford Shale core photos from the northern shelf site, Wyche-1 core. Yellow arrows in the upper Woodford Shale point to phosphate nodules. Core depth tags are measured in feet and inches with a tag every two inches. Approximate depth in meters is posted above each core profile. (For interpretation of the references to colour in this figure legend, the reader is referred to the web version of this article.)

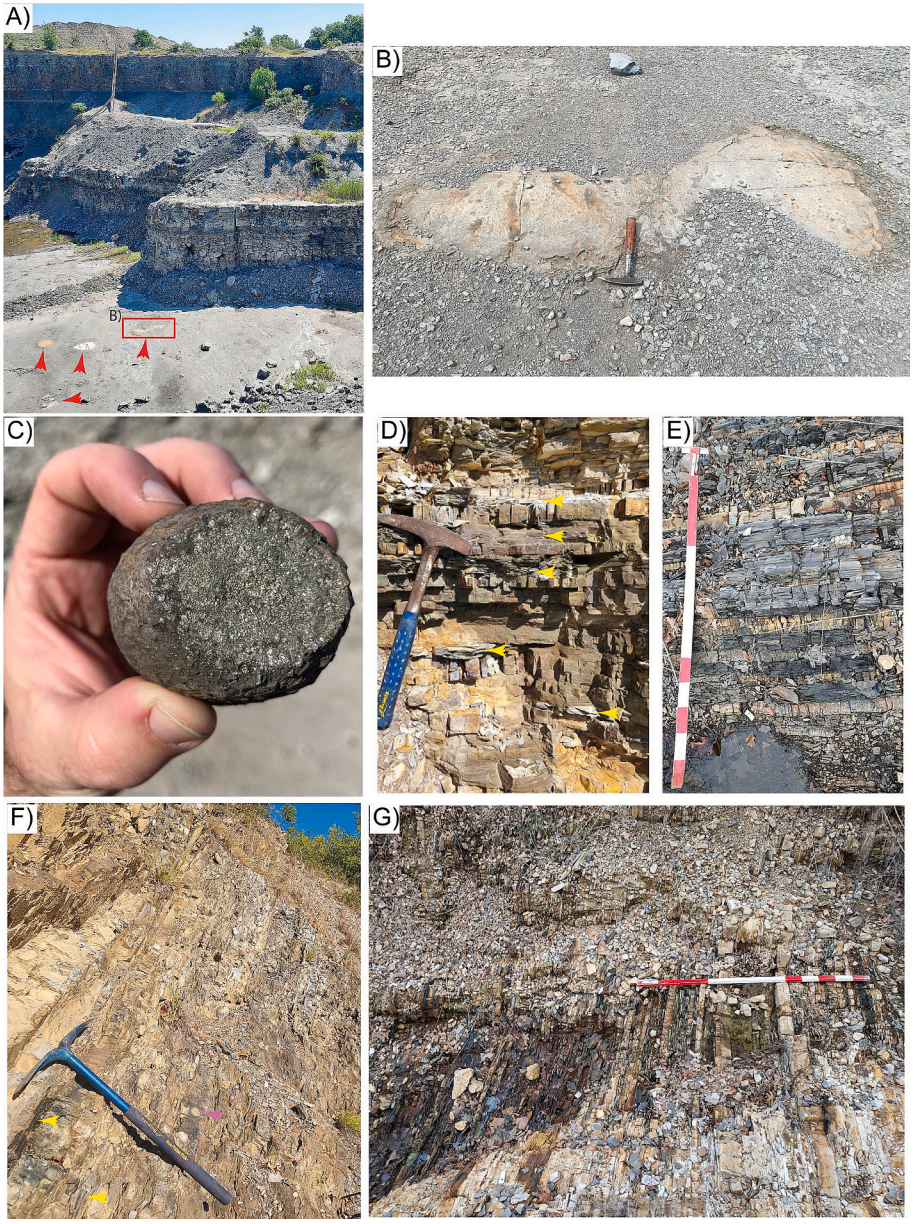

Fig. 4. Representative outcrop photos of the Woodford Shale. A) Wyche Quarry located on the Lawrence Uplift, the site where Wyche-1 core was drilled, northern shelf site. The Quarry mines the upper Woodford Shale, the quarry floor is approximately near the top of the middle Woodford Shale to approx. Basal upper Woodford (Cullen and Hull, 2023). Green arrows point to large concretions of pyrite. The grey box outlines the concentration that is shown in photo insert B. B) Large concentration mostly comprised of pyrite. Small circular to oblong features within the concentration are phosphate nodules. C) Spherical pyrite nodules that can be found within some Woodford Shale outcrops. D) Upper Woodford Shale at I35-south outcrop section, southern shelf site, displaying alternating characteristics of argillaceous mudstones (yellow arrows) and highly siliceous mudstones. The argillaceous mudstones were preferentially selected for geochemical analysis. E) Argillaceous mudstone and highly siliceous cherty mudstone in the Lower to middle Woodford Shale at Hass-B outcrop section, the lower portion of the southern shelf site. F) Near the top of the upper Woodford Shale at the southern shelf site, I35-south section, that is biostratigraphically constrained to be within the l. *praesulcata* – l. *expanasa* conodont zonation. Note the increase in thickness and frequency of cherty highly siliceous mudstone layers vs the very thin argillaceous mudstone layers, yellow arrows. The argillaceous mudstone layers at this section of the outcrop were also only sampled for geochemical analysis. Purple arrow points to phosphate nodule. G) Outcrop section of the Hass-B, southern shelf site approximately around the Frasnian – Famennian boundary. Note there is no macroscopic, outcrops scale difference across the Frasnian – Famennian boundary. (For interpretation of the references to colour in this figure legend, the reader is referred to the web version of this article.)

thicken basinward (southward; Fig. 2; Over, 1990). On the Lawrence Uplift the Frasnian section is only ~20 cm thick (Hass-En site, see fig. 15 in Over, 1990) while correlative sections on the southern shelf range from ~12–15 m thick (Fig. 2; Over, 1990).Thickness variations of the Frasnian sections reflect an overall transgressive on-lap and in-filling of irregular karstic paleotopography of the underlying Hunton Limestone (Amsden, 1975; Infante-Paez et al., 2017; Zhang and Slatt, 2019). The youngest reported conodont zone in the lower Woodford Shale is the early Famennian upper *Palmatolepis triangularis*. Conodonts recovered from the upper Woodford Shale accumulation during the late Famennian to early Tournaisian at least between the *Palmatolepis gracilis expanasa*, to *Siphonodella duplicata* conodont zones. Schwartzapfel and Holdsworth (1996) used radiolaria to place the upper Woodford Shale in the Late Famennian *Holoeciscu 3* – to Tournaisian *Albaillella 1* radiolarian zones. Kondas et al. (2018) similarly reported that the Upper Woodford extends into the middle Tournaisian *VI* – *HD* miospore zones.

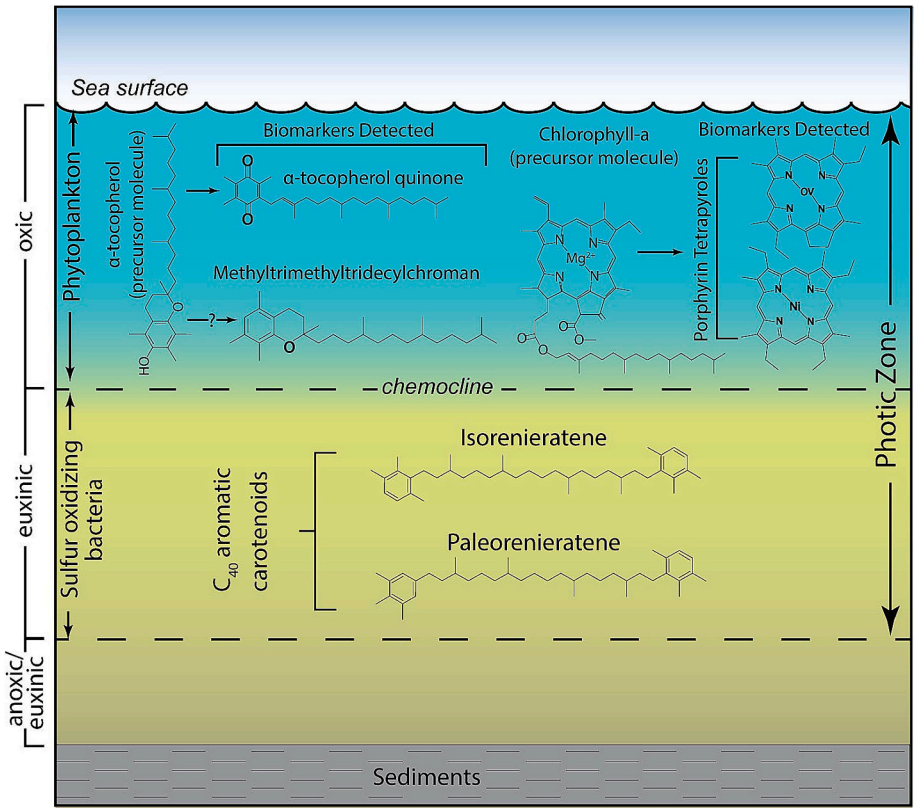

Fig. 5. Conceptual water column redox profile with associated precursor molecules and detected lipid biomarkers.

2.3. Tectonic and depositional settings

Late Proterozoic through Paleozoic regional tectonics controlled deposition of Paleozoic strata in the study area. The Southern Oklahoma Aulacogen (SOA) formed as a failed rift system during the Late Proterozoic-Cambrian along the southern Laurussian passive margin. Outside of the SOA, extensional tectonism left a structural fabric of high-angle normal faults and horst-graben structures including the Lawrence Uplift in central Oklahoma and the Franks Graben to the south (Fig. 2; Mairs, 1966). Post-rift thermal subsidence within the SOA enabled accumulation of a thick succession of Cambro-Ordovician carbonate and sandstone. Although subsidence rates waned from the Silurian to-Mississippian (Feinstein, 1981) they enabled accumulation of the Woodford Shale across a passive margin that faced the Rheic Ocean. Closure of the Rheic Ocean during the Alleghanian – Ouachita orogenies and uplift of the Ancestral Rockies (Kluth, 1986) initiated contractional deformation lasting from the latest Mississippian to the early Permian (Perry, 1989). Inverted rift-related faults of the SOA formed the Wichita-Amarillo-Arbuckle Uplifts and flexurally loaded the Anadarko Basin (Johnson et al., 1989).

2.4. Woodford Shale outcrops presented in this study

The Woodford Shale crops out on the Lawrence Uplift and along Late Paleozoic deformation belts including the Arbuckle Uplift, Criner Hills Uplift, and the Ouachita fold-thrust-belt (Fig. 2). In this study outcrops on the Lawrence Uplift are referred to as the "northern shelf," whereas outcrops along deformation belts are termed "southern shelf."

The Wyche Quarry is an active quarry located on the Lawrence Uplift. The Wyche-1 core is ~64 m long and was drilled behind the quarry wall. Rock Eval and organic geochemistry data indicate that the strata here are thermally immature (Romero and Philp, 2012; Connock et al., 2018). Although the core lacks biostratigraphic analysis, multiple locations on the Lawerence Uplift with conodont biostratigraphy (Over, 1990, 1992) indicate that the northern shelf site is of primarily Famennian age (with possible Tournaisian strata in the uppermost part; Cullen and Hull, 2023). For simplicity, the paleogeographic location of Wyche-1 will be referred to as the "northern shelf site" in this study.

The Arbuckle Mountains, which represent southern shelf Woodford Shale outcrops, are ~54 km southeast from the northern shelf site. Thermal maturity of the Woodford Shale within the Arbuckle Mountains ranges from immature to marginally mature (Cardott and Chaplin, 1993). Outcrop exposures of the Woodford Shale are located on the north and south limbs of the uplift (Fig. 2). The Hass-B outcrop is located on the north limb of the Arbuckle Mountains and captures the lower – middle Woodford Shale encompassing the Frasnian – Famennian transition (Fig. 2; Over, 1990; Crick et al., 2002). The I35-south outcrop is located on the southern limb of the Arbuckle Mountains (Fig. 2). The I35-south section represents the middle – upper Woodford Shale (Becerra et al., 2018). Here, the upper Woodford Shale contains chert layers intercalated with laminated shale (Fig. 4F). Near the top of this outcrop section, a ~ 4 m biostratigraphically constrained interval captures the Famennian – Tournaisian transition (Over, 1990). Famennian conodonts from this section include lower *Palmatolepis gracilis expanasa* – lower *Siphonodella praesulcata* zones, thus the interval of late Devonian Gondwanan glaciation. Palynological data also place the Famennian-Tournaisian boundary within the upper Woodford at this site (Kondas et al., 2018). For simplicity, the paleogeographic location of the outcrops in the Arbuckle Mountains are termed the "southern shelf site" and presented as one composite section (Fig. 2).

2.5. Geochemical background: iron speciation, molybdenum and vanadium as paleoredox indicators

The oxygenation state of marine waters exerts an influence on both the solubility of metals and the preservation of organic carbon. Therefore, many metals serve as paleoredox proxies for ancient marine depositional environments. Fe speciation is widely used to indicate local

marine bottom water redox conditions in organic-rich shales. Fe speciation involves detecting Fe enrichments through the ratios of Fe_T/Al and Fe_{HR}/Fe_T, where the latter provides insights on the degree of anoxia (Raiswell et al., 2001, 2018; Poulton, 2021). To detect total Fe enrichment, values of Fe_T/Al above the Paleozoic Shale average of $Fe_T/Al = 0.53$ (Raiswell et al., 2008), are empirically considered to be enriched in Fe, while values below 0.53 are Fe depleted (Raiswell et al., 2018). Fe_{HR}/Fe_T detects enrichments of the highly reactive iron species relative to the total iron pool, which serves as a measure of anoxia (Poulton and Canfield, 2011; Raiswell et al., 2018; Poulton, 2021). Low values (0–0.22) of Fe_{HR}/Fe_T indicate oxygenated waters whereas values >0.38 indicate anoxic bottom waters. Intermediate values (0.22–0.38) represent possible anoxia. Iron speciation can further reveal whether anoxic environments were ferruginous (free $Fe^{2+}_{(aq)}$) or euxinic (free H_2S) by Fe_{py} normalized to Fe_{HR} (Raiswell et al., 2018; Poulton, 2021). Fe_{py}/Fe_{HR} values below 0.60 indicate ferruginous conditions whereas Fe_{py}/Fe_{HR} of 0.80 to 1.00 represents euxinic environments (Poulton, 2021). Intermediate values of Fe_{py}/Fe_{HR} (0.60 to 0.80) indicate possible euxinic bottoms waters or a weakly sulfidic environment (Poulton, 2021).

The use of the transition metals molybdenum (Mo) and vanadium (V), integrated with Fe speciation, serves as an additional indicator for paleoredox conditions. Mo is particularly useful for detecting sulfidic environments (Tribovillard et al., 2006). It is soluble in oxic seawater and exists in the species molybdate (MoO_4^{2-}). Oxic environments can sequester Mo into sediments by adsorption of Mo onto manganese (Mn) (oxyhydr-)oxides during deposition. However, Mo concentrations in sediments are greatly increased under euxinic conditions as Mo reacts with sulfides to form thiomolybdate ($MoO_xS_{4-x}^{2-}$). While there are several pathways for Mo to be sequestered under euxinic conditions, it is commonly associated with organic matter and pyrite (Phillips and Xu, 2021). Concentrations of Mo that range from 20 to 100 ppm indicate at least intermittent euxinia, whereas values >100 ppm imply persistent euxinia (Scott et al., 2017). Unlike Mo, V does not require the presence of free sulfides to be sequestered within marine sediments. Rather, V is sensitive to suboxic, anoxic, and euxinic redox environments, thus the initial reduction of V occurs under low-oxygen conditions and is not dependent upon the presence of sulfide, and thus has been used to indicate changes in local reducing conditions when paired with other proxies that can track sulfidic conditions (Owens et al., 2016; Kozik et al., 2023). Vanadium undergoes reduction to V(IV), producing compounds like vanadyl ions (VO_2^+) or hydroxyl species (e.g., $VO(OH)^{3-}$) under suboxic to anoxic conditions. These forms of vanadium can accumulate in sediments via surface adsorption or by creating organometallic complexes. When conditions become more strongly reducing (e.g., anoxic + free hydrogen sulfide = euxinic), V experiences further reduction to V(III), potentially precipitating as oxide (V_2O_3) or hydroxide ($V(OH)_3$) phases (Algeo and Maynard, 2004; Owens et al., 2016).V concentrations above 97 ppm imply redox environments of at least suboxic to anoxic (Rudnick and Gao, 2003).

3. Methods

3.1. Sample selection and sample quality control

Samples ($n = 43$) of the Woodford Shale were analyzed from both the northern and southern shelf sites to characterize the inorganic and organic geochemistry on the shelf. Since the upper Woodford Shale at the southern shelf site contains chert layers intercalated with laminated shales (Fig. 4F), samples for geochemical analysis were extracted from the shale layers. Lithofacies descriptions for the northern shelf site are reported in Turner et al. (2015). Detailed lithofacies for southern shelf site are reported in Aufill (2007) for Hass B outcrop section and Becerra et al. (2018) for the I-35 south outcrop section.

To minimize weathering signatures, outcrop surface exposures were excavated down several centimeters and samples were trimmed with a rock saw to expose fresh surfaces and assess the extent of weathering. Both outcrop and core samples were washed and brushed under running deionized (DI) water and inspected under a binocular microscope. Samples for inorganic and organic geochemistry were powdered using an agate mortar and pestle. Silica gel powder was ground within the mortar and pestle and rinsed with DI water between each sample.

3.2. Geochemistry methods

3.2.1. Total organic carbon

Approximately 15–18 mg of dry powdered sediment was placed in silver capsules for total organic carbon measurement. Following published methods (Nieuwenhuize et al., 1994; Brodie et al., 2011), repeated acid addition followed by heating was used to remove inorganic carbon from samples prior to measurement of total organic carbon. Each sample was initially introduced to 10 μL of ultra-pure water followed by 5 μL of 0.1 N HCl. Two subsequent rounds of 5 μL of 6 N HCl and heating the samples to 50 °C were done. Total organic carbon values were measured on an Elementar Vario EL Cube elemental analyzer (Elementar Americas, Ronkonkoma, NY, USA) with check standards of sulfanilamide every 15 samples. All sulfanilamide samples remained at 41.81 % carbon, indicating an instrument precision of +/− 0.01 %.

3.2.2. Iron speciation

We analyzed the highly reactive iron species (Fe_{HR}) as an indicator of local paleoredox conditions, and as a proxy for the iron that may have been bioavailable during the time of deposition of the Woodford Shale. Measurements of Fe_{carb}, Fe_{ox}, and Fe_{mag} were obtained by sequential iron extraction (Poulton and Canfield, 2005; Poulton and Raiswell, 2005). Approximately 100 mg of dry powdered sediment, from grey to black organic-rich marine shales, was placed into 15 mL centrifuge tubes followed by the addition of 10 mL of a reactant solution and agitated for a prescribed duration. Fe_{carb} was obtained by the addition of sodium acetate buffered with acetic acid, pH of 4.5, and agitated between 30 and 48 h. Fe_{ox} was extracted through a reagent of sodium dithionite buffered with acetic acid and sodium citrate, pH of 4.5, and agitated for 2 h. Fe_{mag} was obtained using 10 mL of ammonium oxalate buffered with ammonium hydroxide, pH of 3.2, and agitated for 6 h. Between each step following agitation, 5 mL of the supernatant was pipetted into a 15 mL centrifuge tube while the remaining 5 mL was decanted as waste before adding the following reagent. The iron concentrations of the extracted residues were diluted and measured using an Agilent 7500cs quadrupole inductively coupled plasma mass spectrometer (ICP-MS) in the Geochemistry Group at the National High Magnetic Field Laboratory at the Florida State University.

Iron pyrite (Fe_{py}) concentrations were gravimetrically derived through a chromium-reducible sulfur (CRS) method (Canfield et al., 1986). A solution of 65 mL of 12 M HCl and 135 mL of 1 M $CrCl_2$ was introduced to Zn(s) pellets. The solution was titrated at ~1–2 drops per second into a tri-neck flask containing ~500 mg of dry powdered sediment. The reaction liberates sulfur from pyrite by evolving $H_2S(g)$ from the sediment. Due to the highly-reactive nature of $H_2S(g)$ in an oxidizing environment the reaction was carried out in an anoxic environment with N2(g) headspace. The liberated $H_2S(g)$ from the sedimentary pyrite rises through a condensing tower and passes through a solution of sodium citrate which scrubs carbonate ions and $Cl_2(g)$, and the remaining gas is subsequently bubbled into a solution of $AgNO_3(l)$ whereby $Ag_2S(s)$ is precipitated. The concentration of $Fe_{(py)}$ is stoichiometrically derived from the mass of the precipitated $Ag_2S(s)$ with respect to the initial mass of powdered sediment.

3.2.3. Total digest for trace metal analysis

Trace metals are commonly sequestered in marine sediments with organic matter and provide insights on the local to global marine redox conditions. To determine total concentrations of metals, such as Fe, Al, Mo, and V, a total digest procedure was conducted on 43 samples. Approximately 100 mg of powdered sediment was placed in ceramic

crucibles and combusted at 400 °C for ~8 to 12 h to remove volatile organic matter. Samples were subsequently transferred to Teflon beakers and introduced to a series of several trace metal grade acids (HCl, HNO_3, and HF) in various concentrations and mixtures until all sediment was completely dissolved in solution. Elemental concentrations were obtained using the same Agilent 7500cs quadrupole ICP-MS described above for the Fe speciation analyses. The USGS reference standard SGR-1, Green River Shale, was analyzed simultaneously. All elements deviated from the known concentration, thus a correction was applied to all standards and samples to account for this difference, with iron (observed = 1.60 wt%; expected = 2.12 wt%), aluminum (observed = 2.79 wt%; expected = 3.45 wt%), molybdenum (observed = 31.56 ppm; expected = 35.10 ppm), and vanadium (observed = 112.92 ppm; expected = 128.0 ppm) values for SGR-1 being −24 %, −19 %, −10 %, and − 12 % respectively (See supplemental file). There are a few Fe_{HR}/Fe_T data points that range > 1, reflecting compounding errors from the multiple steps for the Fe extraction.

It is worth noting that we directly measure metal contents using whole rock geochemistry rather than estimating them using handheld X-ray fluorescence (XRF) techniques as was done for most prior studies of the Woodford Shale (see Slatt et al., 2018). For Mo in the Woodford Shale, Pew (2021) reported an r^2 correlation coefficient of 0.47 between XRF and ICP-MS techniques which suggests the former method is not robust for making detailed redox and paleoenvironmental interpretations.

3.2.4. Total lipid extractions, detection, and quantification

Samples ($n = 24$) from the southern shelf site were analyzed for lipid biomarkers of photosynthesis to measure organic matter contributed by primary producers and to serve as redox proxies. We targeted groups of the C_{40} aromatic carotenoids, vanadyl (VO) and nickel (Ni) porphyrins (C_{31}-C_{33} VO-BiCAP, C_{29}-C_{32} VO-DPEP, C_{29}-C_{32} VO-Etios, C_{31}-C_{33} Ni-BiCAP, C_{29}-C_{32} Ni-DPEP, C_{27}-C_{32} Ni-Etios), α-tocopherol quinone (α-TQ), and Methyltrimethyltridecylchhroman (MTTC) to monitor contributions from primary production. The targeted C_{40} aromatic carotenoids include isorenieratane and paleoreniertane, which are pigments synthesized by anoxygenic planktonic photosynthetic sulfur-oxidizing bacteria such as green sulfur bacteria (GSB) that indicate photic-zone euxinia (Fig. 5; French et al., 2015). Compounds of VO and Ni porphyrins are proxies for primary productivity as these compounds are the degraded relicts of the tetrapyrrole structure of chlorophylls produced by photosynthetic organisms (Fig. 5). The VO^{2+} and Ni^{2+} ions replace the original Mg^{2+} ion within the center of the tetrapyrrole structure during diagenesis. The chelation of VO^{2+} or Ni^{2+} is largely dependent on the redox conditions. VO outcompetes Ni for chelation in the tetrapyrrole structure within anoxic conditions. α-tocopherol quinone serves as another indicator of primary production as it is a degraded isoform of vitamin-E, which is synthesized within thylakoid membranes of photosynthetic organisms for photoprotection (Havaux et al., 2005; Mokrosnop, 2014; Connock and Liu, 2023). While the origin of MTTCs is not completely known, it is thought to be a tocopheral derivative and linked to phytoplankton (Fig. 5; Connock and Liu, 2023).

To extract total lipid biomarkers, we followed a slightly modified procedure outlined in Parks and Liu, 2023. Approximately 0.3–0.5 g of dry powdered shale was used for total lipid extractions. Prior to extractions, 1000 ng of VO-tetraphenylporphyrin (VO-TPP) and *Ni*-tetraphenylporphyrin (Ni-TPP) were injected as standards for VO and Ni metalloporphyrins and 100 ng of C_{46} glycerol trialkyl glycerol tetraether (C_{46} GTGT) were injected as standards for the C_{40} aromatic carotenoids, MTTC and α-tocopherol quinone. A total of four extractions were performed with two different solvents. The first two sets of extractions were achieved through 1.50 mL of 1:1 of dichloromethane: methanol (DCM: MeOH) followed by 20 min of sonication. The third and fourth extraction rounds were achieved through 1.50 mL of acetone followed by 20 min of sonication. Vials containing extracts were dried down with N_2(g) on a hot plate at ~50 °C then redissolved into 2 mL vials in 1 mL of 100 % MeOH.

Biomarkers were identified on an Agilent 1290 UPLC system with Agilent 6530 qTOF. Detection of metalloporphyrins were conducted by the reversed-phase liquid chromatography electrospray ionization quadrupole time-of-flight mass spectrometry RPLC-ESI-qTOF-MS method described in Liu (2023). Peaks of targeted compounds were manually integrated off an extracted ion chromatograph. Biomarker concentrations were calculated based off their respective standards and normalized to TOC. We present new MTTC and α-tocopherol quinone integrated with porphyrins and C_{40} aromatic carotenoids from Parks and Liu (2023) for the northern shelf site. New data set of MTTC, α-tocopherol quinone, carotenoids, and porphyrins generated from this study are reported from the southern shelf composite site.

4. Results

4.1. Geochemical attributes

4.1.1. Northern shelf site (Wyche-1 core)

Total organic carbon varies from 2 to 19 wt%, averaging 8 wt% (σ = 4.41; SE = 1.06; $n = 17$) throughout the section. The most elevated TOC values are in the lower and middle Woodford Shale, and lowest values are in the uppermost Woodford Shale (Fig. 6). Fe_{HR}/Fe_T values at this site are generally moderate to low, 0.17–0.79, averaging 0.38 (σ = 0.19; SE = 0.04; n = 17) (Fig. 6). Weight percent values of Fe_{py}/Fe_{HR} range from 0.48 to 0.96, averaging 0.78 (σ = 0.16; SE = 0.04; n = 17). Fe_T/Al values are generally low to moderate, ranging from 0.26 to 1.15, averaging 0.53 (σ = 0.27; SE = 0.06; n = 17), with some elevated samples in the lower and middle Woodford Shale while the lowest values occur in the upper Woodford Shale (Fig. 5). Molybdenum concentrations span a wide range 6.5–107 ppm, averaging 47.52 ppm (σ = 32.74; SE = 7.94; n = 17) but generally decrease upward. Vanadium values for the northern shelf site fall between 112 and 696 ppm, averaging 224.8 ppm (σ = 156.50; SE = 37.95; n = 17). Vanadium trends generally follow other proxies and have similar inflections points. However, in some instances, the V values are antithetical to the other redox proxies.

The concentration of MTTC and α-tocopherol quinone show a similar stratigraphic trend where abundances greatly increase and peak within the upper Woodford Shale (Fig. 6). As reported in Connock et al. (2018) and Parks and Liu (2023), the lower Woodford contains relatively low concentrations of the C_{40} carotenoids, with a slight elevation near the boundary between the lower and middle Woodford Shale. Peak values of the C_{40} carotenoids occur within the middle Woodford at 44 m. The upper Woodford Shale generally exhibits lower concentrations of both C_{40} aromatic carotenoids. Porphyrins show peaks near the lower – middle Woodford Shale boundary and increase in abundance within the upper Woodford Shale (Fig. 6).

4.1.2. Southern shelf sites (Hass-B and I35-south composite)

Total organic carbon remains elevated at the southern shelf site section ranging from 2 to 24 %, averaging ~13 % (σ = 5.18; SE = 1.01; $n = 26$) (Fig. 7). Fe_{HR}/Fe_T displays a broad distribution of values lacking a clear stratigraphic trend (Fig. 7). Fe_{HR}/Fe_T values overall across the composite section range from 0.18 to 1.13, averaging 0.60 (σ = 0.23; SE = 0.04; n = 26). While Fe_{HR}/Fe_T in the lower and middle Woodford Shale sections is generally >0.40, some values fall between 0.2 and 0.4. Fe_{HR}/Fe_T in the upper Woodford Shale, with the interval near the Devonian-Carboniferous boundary exhibiting the lowest of values. Fe_{py}/Fe_{HR} values are predominantly elevated and show similar patterns to Fe_{HR}/Fe_T. Fe_{py}/Fe_{HR} values fall between 0.09 and 0.98, averaging 0.79 (σ = 0.23; SE = 0.04; n = 26). Most elevated values of Fe_{py}/Fe_{HR} are predominantly in the lower to middle Woodford Shale (from the Hass-B section), ranging from 0.50 to 0.97, averaging 0.83 (σ = 0.14; SE = 0.04; $n = 14$). Overall, ratios of Fe_T to Al show a slight decreasing trend in the upper Woodford Shale. All Fe_T/Al values, excluding the dolomitic bed, range between 0.11 and 1.31, averaging 0.52 (σ = 1.13; SE = 0.22; n =

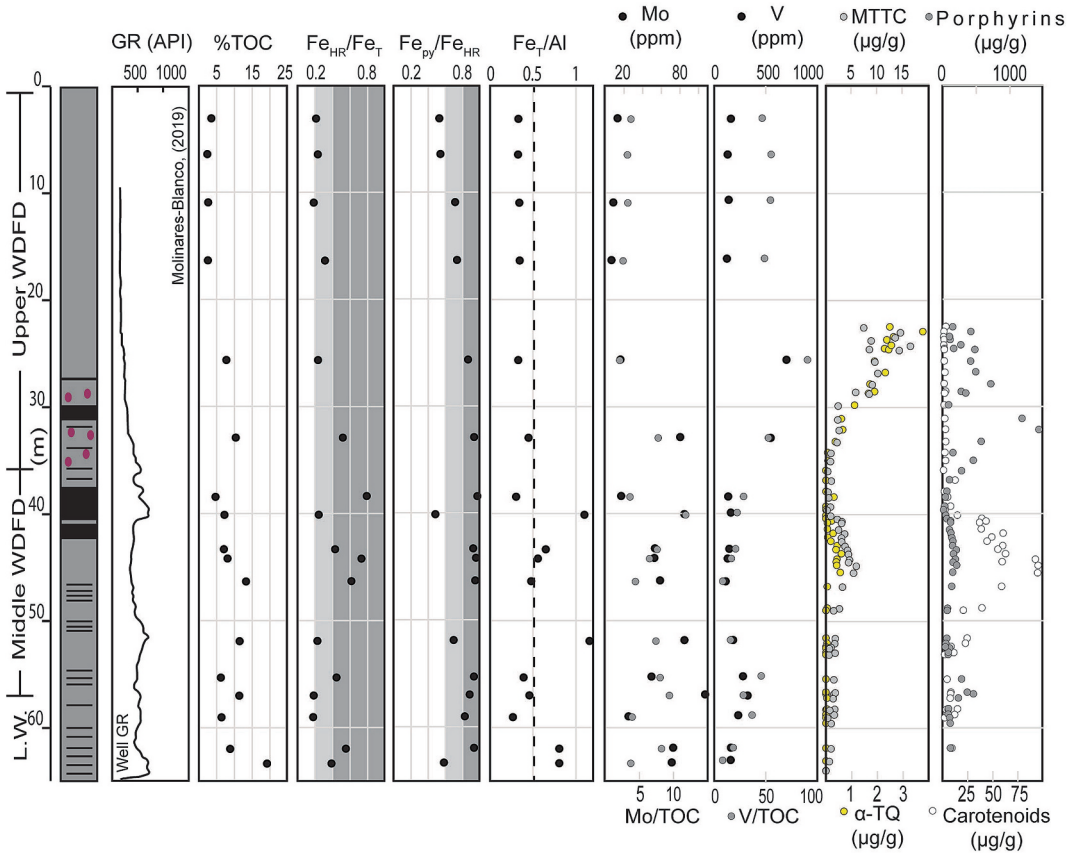

Fig. 6. Geochemical profile of the northern shelf site. The vertical dashed line within Fe_T/Al is the Paleozoic Shale average (0.53; Raiswell and Canfield, 1998). Carotenoids and porphyrins are from Parks and Liu (2023).

26). Mo ranges between ~16 - ~339 ppm, averaging 92 ppm (σ = 67.61; SE = 13.26; n = 26) with the highest values in the middle Woodford Shale and the lowest values in the upper Woodford Shale. Mo concentrations display an overall decreasing trend throughout the stratigraphic section. Mo concentrations generally follow the trend observed in Fe_{py}/Fe_{HR}. Endmember values for V range between 89 and 3786 ppm, averaging 650.91 ppm (σ = 894.51; SE = 175.43; n = 26). V tends to follow the trend of Mo throughout both sections of the southern shelf site.

All biomarkers generally track one another (Fig. 7). MTTC and α-tocopherol quinone within the Frasnian – Famennian section display the highest concentrations whereas they approach 0 µg/g within upper part of the section. These ~0 µg/g values may indicate these biomarkers were either not preserved or their concentrations are lower than detection limits. The detection limit of the analytical method used in this study has been reported previously (see Supplementary Information of Connock et al., 2022). Although we did not determine the exact detection limits for MTTC and α-TQ due to the lack of authentic standards, the general detection limit for most compounds using this method is approximately 0.001 ng. C_{40} aromatic carotenoid abundances overall are lower than those recorded from the northern shelf site. However, the highest values are similar within the lower and middle Woodford Shale. The upper Woodford Shale at this location generally exhibits depleted values with intermittent elevated values. A secondary peak is exhibited in the upper Woodford. Porphyrins display a general upward increasing trend, where they are highest in abundance in both the middle and upper Woodford Shale (>100 µg/g).

5. Discussion

5.1. Total organic carbon and local marine redox

The organic richness of the Woodford Shale, averaging 11 % TOC (this study), is consistent in range and magnitude with values reported by Romero and Philp (2012), Becerra et al. (2018), and Connock et al. (2018). These TOC data record elevated preservation of organic carbon and likely a reflection of both elevated primary productivity and sustained organic carbon preservation—the latter generally linked to oxygen-depleted marine conditions. Any spatial heterogeneity of preserved total organic carbon across the southern Laurussian shelf through time may be enhanced, or diminished, by a number of mechanisms including sedimentation rates, detrital input, and paleo-water depth in addition to the bottom water redox environments. Regardless, the enhanced burial of organic carbon in the Woodford Shale and globally correlative black shales augmented the pCO_2 drawdown attendant with the Devonian expansion of vascular land plants.

5.1.1. Local redox conditions at the northern shelfal site—Wyche-1

Fe_{HR}/Fe_T values between 0.17 and 0.79 suggest that conditions fluctuated between oxic and anoxic at the northern shelf site; however, a predominance of values for $Fe_{HR}/Fe_T > 0.40$, $Fe_{py}/Fe_{HR} > 0.80$ and Mo >25 ppm signal a prevalence of anoxic, and at times euxinic, bottom water conditions. These Fe speciation and Mo geochemical data pointing toward varied redox conditions reinforce observations of alternating redox environments and episodes of strong sulfidic conditions revealed from biomarker paleoredox proxies (Romero and Philp, 2012; Connock et al., 2018; Parks and Liu, 2023). The middle Woodford, which accumulated within Famennian greenhouse conditions, displays some of the strongest anoxic – euxinic conditions. C_{40} aromatic carotenoids also

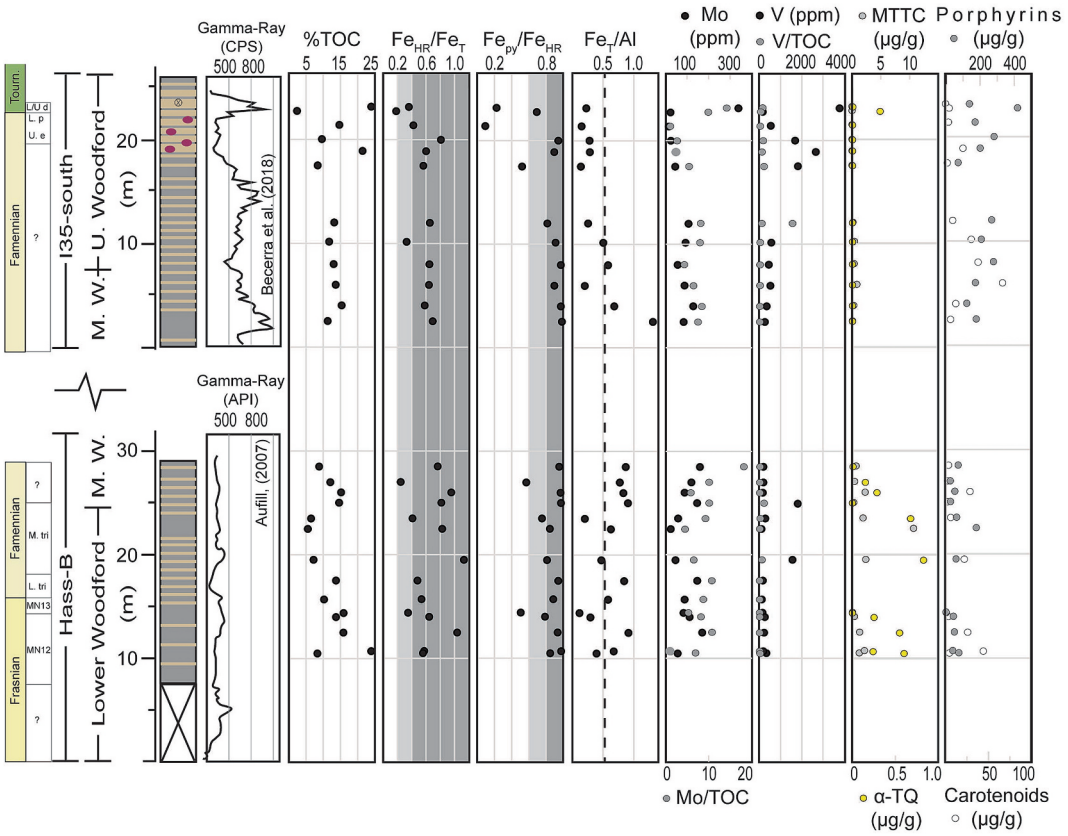

Fig. 7. Geochemical profile for the southern shelf site. The lower portion is from the Hass-B outcrop section on the northern end of the Arbuckle Mountains. The top portion is from the I35-south outcrop section with is from the southern end of the Arbuckle Mountains. The vertical dashed line within Fe_T/Al is the Paleozoic Shale average (0.53; Raiswell and Canfield, 1998). Gamma ray profiles are from Aufill (2007) and Becerra et al. (2018). Designation of lower, middle, upper Woodford are from Cullen and Hull, 2023 and Becerra et al., 2018. Conodont zonations are adapted from Over, 1990 and Crick et al. (2002). Conodont zonation abbreviations are as follows: L. tri – lower *triangularis*; M. tri – middle *triangularis*; U. e – upper *expanasa*; L. p – lower *praesulcata*; L/U d – lower/upper *duplicata*.

support the presence of sulfide within the photic zone. Concentrations of C_{40} aromatic carotenoids in the lower- and upper most Woodford Shale at this northern site may represent short-lived or seasonal development of PZE on the shelf by the end of Woodford Shale deposition. A trend toward lower values of Fe_{HR}/Fe_T, Fe_{py}/Fe_{HR}, and Mo in the upper Woodford Shale supports the idea of less-reducing conditions, which is also reflected in biomarker paleoredox proxies of pristane / phytane (Pr/Ph) and VO/(VO + Ni) porphyrin (Romero and Philp, 2012; Parks and Liu, 2023). However, V concentrations >97 ppm and high V/TOC values (Fig. 6) imply that bottom waters remained overall anoxic. Average Fe_T/Al values (0.53) for all samples within the northern shelf site are consistent with the average Paleozoic Shale values (0.53; Raiswell et al., 2008) and slightly elevated with respect to average upper continental crustal values (0.44; Taylor and McLennan, 1985). The lower and middle Woodford Shale show intervals with elevated Fe while the upper Woodford Shale displays an overall lack of Fe enrichment. Zones where Fe_{HR}/Fe_T values are low but corresponding Fe_{py}/Fe_{HR} values are high, such as the lower – middle contact and the upper Woodford ~25 m, may represent a short-lived shift of the chemocline to within the sedimentary porewaters (Hardisty et al., 2018). However, this interpretation is not entirely certain at the lower – middle Woodford Shale contact since Mo concentrations are >20 ppm and C_{40} aromatic carotenoids are still detected. Alternatively, the modestly enriched Mo concentrations and co-occurrence of C_{40} aromatic carotenoids may reflect episodic pulses of water column euxinia.

5.1.2. Local redox conditions at the southern shelfal sites—Hass-B & I35-south outcrops

At the southern shelf site, Fe_{HR}/Fe_T values are consistent with anoxic bottom water conditions throughout Woodford Shale deposition. The corresponding Fe_{py}/Fe_{HR} values plot predominantly above the euxinic threshold (0.80) with only a few samples falling within possibly euxinic or ferruginous conditions. By the uppermost Woodford Shale, near the Devono-Carboniferous boundary, Fe_{py}/Fe_{HR} and Fe_{HR}/Fe_T values are generally lower, but still display a shifting of the chemocline to within the sediments. The generally elevated Mo concentrations >20–100 ppm are consistent with the Fe speciation indicating sulfidic (to possibly euxinic) conditions at least within pore fluids. Additionally, the detection of C_{40} aromatic carotenoids indicates that sulfate reduction was occurring in the photic zone, which requires euxinic water column conditions. The average Fe_T/Al of ~0.52 for the entire section is comparable to average Paleozoic shale values (0.53; Raiswell et al., 2008). The Fe_T/Al values are generally elevated above the average Paleozoic shale value within the lower and middle Woodford Shale, which may indicate enhanced inputs of reactive Fe during the most reducing conditions, resulting in elevated Fe_{py}/Fe_{HR}. Meanwhile, the lower values of Fe_T/Al below the average Paleozoic shale baseline in the upper Woodford Shale, with corresponding lowered values of Fe_{HR}/Fe_T and Fe_{py}/Fe_{HR}, suggest a contraction of highly reducing conditions and possibly a loss of Fe as the sulfidic conditions were suppressed into the sediments at this time. Elevated Mo and V concentrations with low Fe_{HR}/Fe_T for samples at the top of this section may be an effect of outcrop post-depositional oxidation of pyrite. or could signal sulfidic pore fluids with overlying non-euxinic water column conditions (Hardisty et al., 2018).

5.1.3. Synthesis of local to regional marine redox conditions on the southern Laurussian continental margin

Iron geochemistry, Mo and V concentrations and C_{40} aromatic carotenoid biomarkers all provide independent constraints on local marine redox proxies at various scales (water column vs. sediment) and locations in this region of the Laurussian southern continental margin. Commonalities are a predominance of euxinic conditions and episodes of PZE, particularly within the lower and middle Woodford Shale (Fig. 8). Despite the presence of diagenetic pyrite in the Woodford Shale (Fig. 4) elevated Mo and V trace metal values together with elevated iron speciation (Fe_{py}/Fe_{HR} vs Fe_{HR}/Fe_T) support a predominance of pyrite formation attributable to bottom water euxinia during deposition, even if the overlying water column may have become ferruginous or oxic. While bottom water euxinia prevailed, all sites indicate that the chemocline depth was shifting dynamically during the Late Devonian, with euxinic conditions at times extending into the photic zone, and at other times possibly confined to sediment porewaters with less-reducing or even oxic conditions within the overlying water column (Fig. 8). Intervals with elevated C_{40} aromatic carotenoids reflect water column euxinia in the photic zone which may or may not have extended to bottom waters. Episodes when the sulfidic chemocline may have shifted to sediment porewaters include intervals with lower Fe_{HR}/Fe_T,

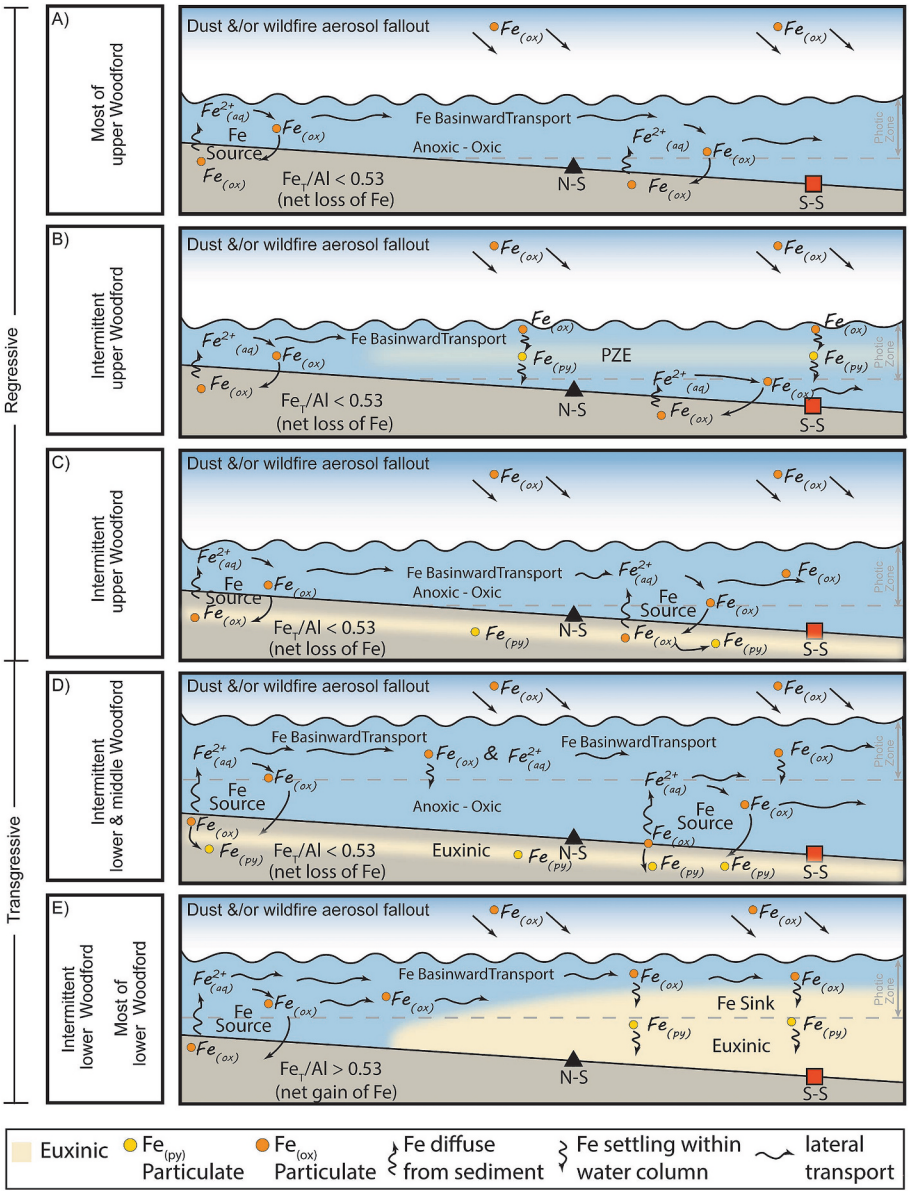

Fig. 8. Conceptual model for the delivery of redox variations and Fe_{HR} delivery on the shelf of the Oklahoma region of the southern Laurentian continental margin. N-S – northern shelf site; S—S – southern shelf site. Models with FeT/Al < 0.53 suggest intervals of active iron loss from sediments to diffuse into overlying water column and shuttled basinward. Intervals with FeT/Al > 0.53 suggest moments when the Woodford Shale acted as an iron sink, trapping Fe in pyrite. The conceptual model is illustrated to show higher sea-level during an overall transgression and lower sea-level during overall regressions. A) Model which characterizes most of the upper Woodford Shale. Less reducing to oxic water column conditions and a net loss of iron from sediments. Iron exported basinward. B) Possible intermittent development of PZE within the water column but bottom waters were non sulfidic allowing a diffusion of Fe from sediments to result in an overall loss of Fe_T. C) Sulfate reducing zone is suppressed within sediment porewaters with an overlying anoxic water column resulting in a net loss of Fe during overall regression. Iron loss from sediments is overall exported basinward D) Sulfate reducing zone is suppressed within sediment porewaters with an overlying anoxic water column resulting in a net loss of Fe during overall transgression. Iron loss from sediments is overall exported basinward. E) Development of euxinia within bottom waters extending into photic zone to characterize most of the middle Woodford Shale and intermittent lower Woodford Shale. Sites at the northern and southern shelf as iron sinks within a possible operating iron shuttle. Model is not drawn to scale.

corresponding with high Fe_{py}/Fe_{HR}, and Mo contents in the multi-tens of ppm (Hardisty et al., 2018), whereas chemoclines within the water column are indicated by elevated Fe_{HR}/Fe_T, Fe_{py}/Fe_{HR}, high enrichments of Mo, and high abundances of C_{40} aromatic carotenoids. The existence of such fluctuations is further bolstered by previous studies documenting intervals of bioturbation and thus bottom-water oxygenation in the Woodford Shale (Coleman and Jordan, 2018). Correlative units, including the Bakken Shale, New Albany Shale and Chattanooga Shale, also record fluctuating redox conditions (Lazar, 2007; Egenhoff and Fishman, 2013; Wilson et al., 2021).

Several mechanisms have been proposed to explain the observed chemocline fluctuations in correlative units of Laurussian basins, including sea-level oscillations and the input of freshwater at proximal sites (Lazar, 2007; Song et al., 2021; Gilleaudeau et al., 2021). For the Chattanooga Shale in the southern Illinois Basin, Song et al. (2021) interpreted deepening of the sulfidic chemocline in the Famennian to reflect overall sea-level fall and the establishment of brackish waters with elevated runoff. The chemocline shifts in the Woodford Shale—especially in the upper Woodford—might similarly record sea-level fluctuations related to far-field effects of glaciation similar to those observed in more proximal environments (Song et al., 2021; Gilleaudeau et al., 2021).

5.2. Models for the delivery of highly reactive iron to the late Devonian southern continental margin of Laurussia

Fe_{py} is the dominant Fe species in the Woodford Shale. Environmental conditions conducive to form pyrite (FeS_2; i.e., euxinia) drove Fe_{HR} enrichments in this shelf system. During euxinic conditions, pyrite formation was limited by the availability of Fe_{HR} [i.e., lithogenic Fe (oxyhrydr)oxides, $Fe^{2+}_{(aq)}$, or Fe(III) bound with organic matter] to react with HS^- or free sulfides (S^{2-}_x) which initially produce iron sulfide (FeS). The iron sulfides later react with H_2S or S^{2-}_x to produce FeS_2 given sufficient TOC and limited available highly reactive Fe species that are not bound as pyrite (Anderson and Raiswell, 2004; Rickard and Luther, 2007).

5.2.1. Iron shuttling

In ancient and modern marine environments, a shelf-to-basin transport system termed the "iron-shuttle" is an effective mechanism to deliver iron across shelves to deep basins (Raiswell and Anderson, 2005; Lyons and Severmann, 2006; Severmann et al., 2008; Scholz et al., 2014, 2019). The process of iron shuttling liberates Fe from reducing sediments, typically as $Fe^{2+}_{(aq)}$, by microbial metabolic processes. During Fe transfer across the shelf along the chemocline, Fe may bond with organic matter, such as organic Fe-bearing ligands, or as Fe_{ox} particulates, which rapidly (minutes to days; Raiswell and Canfield, 1996; Poulton et al., 2004) react with sulfides to form pyrite in euxinic environments. The mobilization of iron from shelf-to-basin is documented as a significant mechanism for the delivery of Fe to Archean oceans and the development of banded iron formations (Severmann et al., 2008; Li et al., 2015; Wang et al., 2024). Today, iron shuttling is the principal mechanism to transfer Fe_{HR} to distal regions of the Black Sea and the Cariaco Basin (Raiswell and Canfield, 1998; Anderson and Raiswell, 2004) and the loss of Fe occurs from modern reducing shelves in the open ocean (Conway and John, 2014).

Iron shuttling may have been active during intervals of Woodford Shale deposition, especially given the dynamic redox conditions on the shelf (Fig. 8). Considering the data presented here, Fe_{HR} was likely sequestered locally when an Fe shuttling processes was active during the deposition of the lower, the middle and the basal upper part of the Woodford Shale. Hence, intervals of deposition where geochemical proxies record euxinia resulted in a net enrichment of Fe, where $Fe_T/Al > 0.53$ (Fig. 8E). Euxinia contributed to developing Fe sinks along the southern Laurussian continental margin study area during the Late Devonian, in the deposition of the lower and middle Woodford Shale. Shifts of the chemocline into sediment pore waters during this time likely enabled intermittent release of Fe from sediment pores, where $Fe_T/Al < 0.53$ (Fig. 8C, D). In contrast, the uppermost Woodford Shale from both sites on the shelf records less-sulfidic environments and overall net losses of Fe, where $Fe_T/Al < 0.53$ (Fig. 8A - C). Deposition of the uppermost Woodford Shale may have largely contributed to diffusing Fe_{HR} from sediment porewaters into overlying anoxic water columns. Thus, during deposition of the youngest Woodford Shale, both sites likely acted as sources for Fe_{HR} shuttling.

Kondas et al. (2018) and Philp and DeGarmo (2020) both noted elevated values of terrigenous organic matter within the upper Woodford Shale, that Kondas et al. (2018) interpreted as a weak regressive signal, consistent with a sea-level fall and presumed onset of icehouse conditions documented by Algeo et al. (2007) in the Late Devonian *Palmatolepis gracilis expanasa – Siphonodella praesulcata* conodont zones (Fig. 1). An elevated flux of terrigenous matter, carrying with it iron predominantly as Fe_{ox}, to the upper Woodford Shale likely contributed additional Fe_{HR}. Algeo et al. (1995) and Algeo and Scheckler (1998) inferred increased nutrient flux into Devonian epeiric seas related to enhanced pedogenesis resulting from the expansion of land plants. Others have posited soil destabilization and erosion attributed to increased wildfires attendant with the expansion of land plants (Kaiho et al., 2013; Philp and DeGarmo, 2020; Lu et al., 2021). Together with the development of more oxidizing bottom water conditions (contraction of highly reducing conditions) and enhanced terrigenous runoff during regressive intervals, Fe supply and source area likely increased, thus enabling Fe shuttling across Devonian epeiric seas. Enhanced pedogenesis, elevated chemical weathering, and terrestrial runoff are also posited to have produced an elevated export of phosphorous, an additional key micronutrient, to Devonian marine environments globally (Algeo et al., 1995; Algeo and Scheckler, 1998). The widespread occurrence of abundant phosphate nodules in the upper Woodford Shale is consistent with a shuttling mechanism of the phosphate cycle (Föllmi, 1996) which may have been operating in conjunction with iron shuttling during this time.

The operation of a late Devonian iron shuttle is not exclusive to the southern Laurussian Woodford Shale system. Shelf-to-basin Fe and Mn particulate shuttles have been documented to facilitate the transfer of Fe from the proximal oxic shelf of the Catskill Delta into an anoxic Appalachian Basin between the middle Devonian to early Carboniferous (Duan et al., 2010; Gilleaudeau et al., 2021). Iron shuttling processes have been documented from modern through Archean marine systems, and it is likely that a shelf-to-basin transfer of bioavailable Fe operated more pervasively as a significant mechanism to help drive primary productivity and the formation of prolific Devono-Carboniferous organic rich shales.

5.2.2. Contributions from the atmosphere — eolian dust and wildfires?

In addition to iron shuttling and other iron sources noted above, Fe_{HR} may be directly delivered from extrabasinal sources rather than riverine input. McGlannan et al. (2022) hypothesized eolian delivery to the marine system for the detrital component of the Woodford Shale as a mechanism to deliver bioavailable iron, given that the system was far removed from deltaic clastic wedges. Today, atmospheric dust from the Sahara supplies the Bahamas, Caribbean, and Amazon with nutrients including Fe and P (Lenes et al., 2001; Swart et al., 2014; Prospero et al., 2020). In the Southern Ocean, recent investigations have demonstrated Fe from dust deposition to be a significant driver of primary productivity (Weis et al., 2024). These processes have been proposed for the Upper Pennsylvanian Horseshoe Atoll in the Midland Basin (Sur et al., 2015) and the Upper Pennsylvanian-Lower Permian Sanan-daj-Sirjan carbonate platform of the Alborz Basin, Iran (Sardar Abadi et al., 2020). These deep-time studies of dust fertilization both show an anomalous signature of elevated Fe_{HR} without an enrichment of the total iron pool (Fe_T), elevated Fe_{HR}/Fe_T with corresponding low Fe_T/Al, suggestive of non-aluminosilicate detrital Fe delivered as Fe (oxyhydr-)oxides (Fe_{ox})

adhered onto clastic dust particles. While the detrital silt in the Woodford Shale and its correlatives is interpreted to have been delivered by wind followed by subsequent marine redistribution (McGlannan et al., 2022), we do not observe a clear geochemical signature of iron fertilization by dust-derived highly reactive iron similar to that documented in Sur et al. (2015) and Sardar Abadi et al. (2020). Rather, Fe_{HR}/Fe_T enrichment in the Woodford Shale and correlatives (Chattanooga, Exshaw, and Bakken) follows the trend of total Fe enrichment (Song et al., 2021; Li et al., 2022; Sahoo et al., 2023). Perhaps the difference reflects in part the contrast in depositional environments between Late Devonian epeiric seas and shallow carbonates in the Permo-Pennsylvanian studies of Sur et al. (2015) and Sardar Abadi et al. (2020). Epeiric seas and continental shelves received Fe_{HR} by multiple processes, (i.e. terrigenous runoff, subaqueous redistribution of sediments, and benthic iron shuttling) in addition to contributions from the atmosphere as opposed to atolls and carbonate platforms where dust is the dominant carrier of Fe_{HR}.

Additional contributions of Fe from the atmosphere may have been promoted by increased wildfire activity that intensified during the late Devonian as a result of the expansion of land plants and the concomitant drawdown of pCO_2 and the rise of pO_2 (Rimmer et al., 2015). Geological evidence of wildfires archived in upper Devonian marine shales has been documented by the occurrence of inertinite macerals transported to marine systems by both runoff and wind in the Appalachian Basin (Rimmer et al., 2015; Liu et al., 2020), the Woodford Shale of southern Laurussia (Cardott and Comer, 2021), and in northern Gondwana (Rahiminejad et al., 2022). Philp and DeGarmo (2020) detected evidence for wildfires in the form of pyrogenic polycyclic aromatic hydrocarbon biomarkers such as such as benzo(*e*)pyrene, benzo(*a*)pyrene, and benzo(*ghi*)perylene with cadelene (Jiang et al., 1998) through a quarried Woodford Shale section. Wildfires aerosolize Fe-bearing soil derived mineral dust from convective winds in addition to subordinate contributions of Fe from the direct combustion of the foliage (Wagner et al., 2018; Perron et al., 2022; Tegler et al., 2023). Aerosols emitted from recent Australian wildfires have promoted significant algal blooms in the Southern Ocean 1000s km downwind of the fire activity (Tang et al., 2021). Perhaps similar processes operated during the Late Devonian.

Whether or not eolian dust and/or wildfire activity played roles in delivery of Fe_{HR} to the Woodford system remains speculative. Any Fe_{HR} delivered from the atmosphere upon settling through the sulfidic water columns of the Late Devonian would have rapidly converted to pyrite within the water column or shortly after deposition within sediment pore waters (Fig. 8), thus, contributing a limited source of Fe_{HR} to sulfide-rich environments to generate Fe_{py} as the dominant Fe species.

5.3. Implications for paleoprimary productivity

While we cannot fully distinguish the relative contributions of productivity and the preservation of organic matter, the trends in biomarkers indicative of primary productivity generally follow the overall trends of water column oxygenation profiles across both the northern and southern shelf sites. Parks and Liu (2023) posited that primary productivity was restricted in the lower and middle Woodford Shale by elevated euxinic conditions but likely became enhanced in the upper Woodford Shale with the onset of a more oxygenated water column, correlating with higher concentrations of porphyrins. Our results from iron geochemistry and biomarkers reinforce this finding.

Throughout Woodford Shale deposition, Fe diffusion from sediment pores was likely the principal mechanism of Fe micronutrient delivery, with possible ancillary contributions from eolian dust and/or wildfires (Fig. 8). During marginally sulfidic conditions Fe is soluble as Fe(II) and in the form of FeS (Rickard, 2006). Therefore, if bottom waters are weakly euxinic, Fe may still diffuse from sediment as a source of bioavailable Fe. While excess H_2S exists under euxinic conditions, burial of Fe_{py} contributed to a net gain of Fe to the Woodford Shale as FeS_2 is insoluble under anoxic condition (Fig. 8). Increased primary productivity requires an increase of nutrients into the system. Elevated loss of Fe diffusing from sediments into overlying less-reducing-to-oxic water column conditions and the delivery of phosphorous, as evidenced by the occurrence of phosphate nodules, within the upper Woodford Shale corresponding with elevated porphyrins, MTTC and α-tocopherol quinone (Figs. 6, 7) implies enhanced nutrient delivery to the Woodford Shale system.

6. Conclusion

- High levels of organic productivity recorded in the Late Devonian black shales of North America, including the Woodford Shale, require an abundant supply of key nutrients —notably iron.
- Iron and biomarker data from the lower and middle Woodford Shale record fluctuations between anoxic and euxinic conditions that indicate a dynamic chemocline. The overall transgressive marine waters during deposition of the lower to middle Woodford Shale were largely euxinic, whereas the overall regressive upper Woodford Shale was less reducing and potentially oxic.
- These fluctuations may record far-field effects of the growth (cooling) and loss (warming) of continental ice during the Late Devonian.
- Throughout Woodford Shale deposition, iron shuttling processes and diffusion of Fe from sediment pore waters was the primary source of Fe delivery, potentially enhanced by wildfires, and delivery of dust.
- The upper Woodford Shale records an overall loss of Fe from sediments which likely contributed to an increased flux of Fe into the overlying water column, thus helping drive increased primary productivity.

CRediT authorship contribution statement

Austin J. McGlannan: Writing – original draft, Writing – review & editing, Conceptualization, Formal analysis, Methodology, Investigation, Visualization. **Jeremy D. Owens:** Writing – review & editing, Resources, Validation, Methodology, Conceptualization, Supervision, Funding acquisition. **Seth A. Young:** Writing – review & editing, Resources, Funding acquisition, Supervision. **Sean M. Newby:** Writing – review & editing, Validation, Investigation, Supervision. **Derek Parks:** Investigation. **Xiao-Lei Liu:** Writing – review & editing, Methodology, Supervision, Funding acquisition, Resources. **Caitlin Hodges:** Writing – review & editing, Resources. **Andrew Cullen:** Writing – review & editing. **Gerilyn S. Soreghan:** Writing – review & editing, Methodology, Resources, Funding acquisition, Supervision, Conceptualization, Project administration.

Declaration of competing interest

The authors declare no known competing interest financially or personally.

Acknowledgments

This paper forms part of A. McGlannan's PhD dissertation, supervised by G. Soreghan. We thank the University of Oklahoma (Soreghan and Hodges) and the Eberly Family Chair and McCollough Chair (Soreghan), the NASA Exobiology Program (80NSSC23K0346 – Owens and Young) (80NSSC22K1559 – Liu), the National Science Foundation (EAR2026926 – Owens), and the Alfred P. Sloan Foundation – Owens for funding. Maya Roselli and Merid Schwartz assisted with processing samples for CRS at Florida State University. Tiffany Legg Ramsel, Benjamin Matsumura, Brittany Moehnke and Jacob Clements greatly assisted with processing samples for total organic carbon. We thank Claire Curry with the University of Oklahoma Libraries and Mehrdad Sardar Abadi for helpful discussions. The Wyche-1 core was drilled as a research core in 2009 in collaboration between the University of

Oklahoma's Institute for Reservoir Characterization, Devon Energy and Schlumberger. We also thank the reviewers and editor for their constructive comments toward the improvement of this manuscript.

Data availability

Data will be made available on request.

References

Algeo, T.J., Maynard, J.B., 2004. Trace-element behavior and redox facies in core shales of Upper Pennsylvanian Kansas-type cyclothems. Chem. Geol. 206, 289–318. https://doi.org/10.1016/j.chemgeo.2003.12.009.

Algeo, T.J., Scheckler, S.E., 1998. Terrestrial-marine teleconnections in the Devonian: links between the evolution of land plants, weathering processes, and marine anoxic events. Philos. Trans. R. Soc. Lond. B Biol. Sci. 353, 113–130.

Algeo, T.J., Berner, R.A., Maynard, J.B., Scheckler, S.E., 1995. Late Devonian oceanic anoxic events and biotic crises: "rooted" in the evolution of vascular land plants. GSA Today 5, 45.

Algeo, T.J., Scheckler, S.E., Maynard, J.B., 2001. Effects of the Middle to late Devonian spread of vascular land plants on weathering regimes, marine biotas, and global climate. In: Gensel, P.G., Edwards, D. (Eds.), Plants invade the land. Columbia University Press, pp. 213–236. https://doi.org/10.7312/gens11160-013.

Algeo, T.J., Lyons, T.W., Blakey, R.C., Over, D.J., 2007. Hydrographic conditions of the Devono–Carboniferous North American Seaway inferred from sedimentary Mo–TOC relationships. Palaeogeogr. Palaeoclimatol. Palaeoecol. 256, 204–230. https://doi.org/10.1016/j.palaeo.2007.02.035.

Amsden, T.W., 1975. Hunton Group (late Ordovician, Silurian, and early Devonian) in the Anadarko Basin of Oklahoma. Oklahoma Geological Survey Bulletin 121, 213.

Anderson, T.F., Raiswell, R., 2004. Sources and mechanisms for the enrichment of highly reactive iron in euxinic Black Sea sediments. Am. J. Sci. 304, 203–233.

Aufill, 2007. Outcrop-Based Correlation of Magnetic Susceptibility with Spectral Gamma-Ray Spectrometry in the Woodford Shale of South-Central Oklahoma [MS Thesis]:. Oklahoma State University, Stillwater, p. 244.

Becerra, D., Galvis, H., Slatt, R., 2018. Characterizing the two principal rock types comprising the Woodford Shale resource play: Application to shale geomechanics. Interpretation 6, SC67–SC84. https://doi.org/10.1190/INT-2017-0146.1.

Blakey, R.C., 2013. North American Key Time Slices © 2013. Colorado Plateau Geosystems, Inc.

Boucot, A.J., Xu, C., Scotese, C.R., Morley, R.J., 2013. Phanerozoic Paleoclimate: an atlas of lithologic indicators of climate. In: SEPM, Concepts in Sedimentology and Paleontology, no. 11, p. 478.

Brezinski, D.K., Cecil, C.B., Skema, V.W., Stamm, R., 2008. Late Devonian glacial deposits from the eastern United States signal an end of the mid-Paleozoic warm period. Palaeogeogr. Palaeoclimatol. Palaeoecol. 268, 143–151. https://doi.org/10.1016/j.palaeo.2008.03.042.

Brezinski, D.K., Cecil, C.B., Skema, V.W., Kertis, C.A., 2009. Evidence for long-term climate change in Upper Devonian strata of the Central Appalachians. Palaeogeogr. Palaeoclimatol. Palaeoecol. 284, 315–325. https://doi.org/10.1016/j.palaeo.2009.10.010.

Brezinski, D.K., Cecil, C.B., Skema, V.W., 2010. Late Devonian glaciogenic and associated facies from the central Appalachian Basin, eastern United States. Geol. Soc. Am. Bull. 122, 265–281. https://doi.org/10.1130/B26556.1.

Brodie, C.R., Leng, M.J., Casford, J.S.L., Kendrick, C.P., Lloyd, J.M., Yongqiang, Z., Bird, M.I., 2011. Evidence for bias in C and N concentrations and δ13C composition of terrestrial and aquatic organic materials due to pre-analysis acid preparation methods. Chem. Geol. 282, 67–83. https://doi.org/10.1016/j.chemgeo.2011.01.007.

Campbell, J.A., Mankin, C.J., Scwarzkopf, A.B., Raymer, J.H., 1988. Habitat of petroleum in Permian rocks of the midcontinent region. In: Morgan, W.A., Babcock, J.A. (Eds.), Permian Rocks of the Midcontinent: SEPM, Midcontinent Section, Special Publication, vol. 1, pp. 13–35.

Canfield, D.E., Raiswell, R., Westrich, J.T., Reaves, C.M., Berner, R.A., 1986. The use of chromium reduction in the analysis of reduced inorganic sulfur in sediments and shales. Chem. Geol. 54, 149–155.

Cardott, B.J., Chaplin, J.R., 1993. Guidebook for Selected Stops in the Western Arbuckle Mountains, Southern Oklahoma. Oklahoma Geological Survey Special Publication, 93-3, 55 p.

Cardott, B.J., Comer, J.B., 2021. Woodford Shale (Upper Devonian to lower Mississippian): from hydrocarbon source rock to resevior: Oklahoma Geological Survey. Bulletin 152, 108. https://www.ou.edu/ogs/publications/bulletins.

Cohen, K.M., Finney, S.C., Gibbard, P.L., Fan, J.-X., 2013. The ICS International Chronostratigraphic Chart, Updated (v. 2021). Episode 36, 199–204.

Coleman, S.M., Jordan, D.W., 2018. Correlation of chemostratigraphy, total organic carbon, sequence stratigraphy, and bioturbation in the Woodford Shale of south-Central Oklahoma. Interpretation 6 p.SC43-SC54.

Comer, J.B., 1992. Organic Geochemistry and paleogeography of Upper Devonian formations in Oklahoma and Northwestern Arkansas. In: Johnson, K., Cardott, B.J. (Eds.), Source Rocks in the southern midcontinent: Oklahoma Geological Survey, Circular, 93, pp. 70–93.

Connock, G.T., Liu, X.-L., 2023. Tocopherols and associated derivatives track the phytoplanktonic response to evolving pelagic redox conditions spanning Oceanic Anoxic Event 2. Geobiology 21, 743–757. https://doi.org/10.1111/gbi.12570.

Connock, G.T., Nguyen, T.X., Philp, R.P., 2018. The development and extent of photic-zone euxinia concomitant with Woodford Shale deposition: American Association of Petroleum Geologist. Bulletin 102, 959–986.

Connock, G.T., Owens, J.D., Liu, X.L., 2022. Biotic induction and microbial ecological dynamics of Oceanic Anoxic Event 2. Communicat. Earth & Environ. 3, 136.

Conway, T.M., John, S.G., 2014. Quantification of dissolved iron sources to the North Atlantic Ocean. Nature 511, 212–215.

Crick, R.E., Ellwood, B.B., Feist, R., El Hassani, A., Schindler, E., Dreesen, R., Over, D.J., Girard, C., 2002. Magnetostratigraphy susceptibility of the Frasnian/Famennian boundary. Palaeogeogr. Palaeoclimatol. Palaeoecol. 181, 67–90.

Cullen, A.B., Hull, D., 2023. An Atlas of Woodford Shale Outcrops in Southern Oklahoma: Oklahoma Geological Survey. Guidebook 40, 196.

Dahl, T.W., Arens, S.K., 2020. The impacts of land plant evolution on Earth's climate and oxygenation state–an interdisciplinary review. Chem. Geol. 547, 119665.

Duan, Y., Severmann, S., Anbar, A.D., Lyons, T.W., Gordon, G.W., Sageman, B.B., 2010. Isotopic evidence for Fe cycling and repartitioning in ancient oxygen-deficient settings: examples from black shales of the mid-to-late Devonian Appalachian basin. Earth Planet. Sci. Lett. 290, 244–253.

Egenhoff, S.O., Fishman, N.S., 2013. Traces in the dark: sedimentary processes and facies gradients in the upper shale member of the Upper Devonian-lower Mississippian Bakken Formation, Williston Basin, North Dakota, USA. J. Sediment. Res. 83, 803–824.

Feinstein, S., 1981. Subsidence and thermal history of southern Oklahoma aulacogen: implications for petroleum exploration: American Association of Petroleum Geologists. Bulletin, v. 65, 2521–2533.

Föllmi, K.B., 1996. The phosphorus cycle, phosphogenesis and marine phosphate-rich deposits. Earth Sci. Rev. 40, 55–124.

French, K.L., Rocher, D., Zumberge, J.E., Summons, R.E., 2015. Assessing the distribution of sedimentary C 40 carotenoids through time. Geobiology 13, 139–151.

Galvis, H., Becerra, D., Slatt, R., 2018. Lithofacies and stratigraphy of a complete Woodford Shale outcrop section in South Central Oklahoma: Geologic considerations for the evaluation of unconventional shale reservoirs. Interpretation 6 p.SC15-SC27.

Geider, R.J., La Roche, J., 1994. The role of iron in phytoplankton photosynthesis, and the potential for iron-limitation of primary productivity in the sea. Photosynth. Res. 39, 275–301.

Gilleaudeau, G.J., Algeo, T.J., Lyons, T.W., Bates, S., Anbar, A.D., 2021. Novel watermass reconstruction in the early Mississippian Appalachian Seaway based on integrated proxy records of redox and salinity. Earth Planet. Sci. Lett. 558, 116746.

Gledhill, M., Buck, K.N., 2012. The organic complexation of iron in the marine environment: a review. Front. Microbiol. 3, 18807.

Hardisty, D.S., Lyons, T.W., Riedinger, N., Isson, T.T., Owens, J.D., Aller, R.C., Rye, D.M., Planavsky, N.J., Reinhard, C.T., Gill, B.C., Masterson, A.L., 2018. An evaluation of sedimentary molybdenum and iron as proxies for pore fluid paleoredox conditions. Am. J. Sci. 318, 527–556.

Havaux, M., Eymery, F., Porfirova, S., Rey, P., Dörmann, P., 2005. Vitamin E protects against photoinhibition and photooxidative stress in Arabidopsis thaliana. Plant Cell 17, 3451–3469.

Infante-Paez, L., Cardona, L.F., McCullough, B., Slatt, R., 2017. Seismic analysis of paleotopography and stratigraphic controls on total organic carbon: Rich sweet spot distribution in the Woodford Shale, Oklahoma, USA. Interpretation 5, T33–T47.

Isaacson, P.E., Díaz-Martínez, E., Grader, G.W., Kalvoda, J., Bábek, O., Devuyst, F.X., 2008. Late Devonian–earliest Mississippian glaciation in Gondwanaland and its biogeographic consequences. Palaeogeogr. Palaeoclimatol. Palaeoecol. 268, 126–142.

Jiang, C., Alexander, R., Kagi, R.I., Murray, A.P., 1998. Polycyclic aromatic hydrocarbons in ancient sediments and their relationships to palaeoclimate. Org. Geochem. 29, 1721–1735.

Joachimski, M.M., Buggisch, W., 2002. Conodont apatite $\delta^{18}O$ signatures indicate climatic cooling as a trigger of the late Devonian mass extinction. Geology 30, 711–714.

Joachimski, M.M., Breisig, S., Buggisch, W., Talent, J.A., Mawson, R., Gereke, M., Morrow, J.R., Day, J., Weddige, K., 2009. Devonian climate and reef evolution: insights from oxygen isotopes in apatite. Earth Planet. Sci. Lett. 284, 599–609.

Johnson, K.S., Amsden, T.W., Dennison, R.E., Dutton, S.P., Goldstein, A.G., Roscoe, B., Sutherland, P.K., Thompson, D.M., 1989. Geology of the southern midcontinent: Oklahoma Geological Survey. Special Publication 89, 1–53.

Kaiho, K., Yatsu, S., Oba, M., Gorjan, P., Casier, J.G., Ikeda, M., 2013. A forest fire and soil erosion event during the late Devonian mass extinction. Palaeogeogr. Palaeoclimatol. Palaeoecol. 392, 272–280.

Kirkland, D.W., Denison, R.E., Summer, D.M., Gormly, J.R., 1992. Geology and organic geochemistry of the Woodford Shale in the Criner Hills and western Arbuckle Mountains, Oklahoma. In: Johnson, K., Cardott, B.J. (Eds.), Source Rocks in the Southern Midcontinent: Oklahoma Geological Survey, Circular 93, pp. 38–69.

Kluth, C.F., 1986. Plate Tectonics of the Ancestral Rocky Mountains. In: Peterson, J.E. (Ed.), Paleotectonics and Sedimentation in the Rocky Mountain Region, United States, 41. American Association of Petroleum Geologist, Memoir, pp. 353–369.

Kolber, Z.S., Barber, R.T., Coale, K.H., Fitzwateri, S.E., Greene, R.M., Johnson, K.S., Lindley, S., Falkowski, P.G., 1994. Iron limitation of phytoplankton photosynthesis in the equatorial Pacific Ocean. Nature 371, 145–149.

Kondas, M., Filipiak, P., Paszkowski, M., Pisarzowska, A., Elmore, R.D., Jelonek, I., Kasprzyk, M., 2018. The organic matter composition of the Devonian/Carboniferous deposits (south flank of Arbuckle Anticline, Oklahoma, USA). Int. J. Coal Geol. 198, 88–99.

Kozik, N.P., Young, S.A., Ahlberg, P., Lindskog, A., Owens, J.D., 2023. Progressive marine oxygenation and climatic cooling at the height of the Great Ordovician Biodiversification Event. Glob. Planet. Chang. 227, 104183.

Kuma, K., Nishioka, J., Matsunaga, K., 1996. Controls on iron (III) hydroxide solubility in seawater: the influence of pH and natural organic chelators. Limnol. Oceanogr. 41, 396–407.
Lakin, J.A., Marshall, J.E.A., Troth, I., Harding, I.C., 2016. Greenhouse to icehouse: A biostratigraphic review of latest Devonian-Mississippian glaciations and their global effects. In: Becker, R.T., Königshof, P., Brett, C.E. (Eds.), Devonian Climate, Sea Level and Evolutionary Events: Geological Society of London, Special Publication, vol. 423, pp. 439–464.
Lazar, O.R., 2007. Redefinition of the New Albany Shale of the Illinois Basin: An Integrated, Stratigraphic, Sedimentologic, and Geochemical Study [Ph.D. Dissertation]:. Indiana University, Bloomington, Indiana, p. 363.
Lenes, J.M., Darrow, B.P., Cattrall, C., Heil, C.A., Callahan, M., Vargo, G.A., Byrne, R.H., Prospero, J.M., Bates, D.E., Fanning, K.A., Walsh, J.J., 2001. Iron fertilization and the Trichodesmiumresponse on the West Florida shelf. Limnol. Oceanogr. 46, 1261–1277.
Li, W., Beard, B.L., Johnson, C.M., 2015. Biologically recycled continental iron is a major component in banded iron formations. Proc. Natl. Acad. Sci. 112, 8193–8198.
Li, S., Wignall, P.B., Poulton, S.W., Hedhli, M., Grasby, S.E., 2022. Carbonate shutdown, phosphogenesis and the variable style of marine anoxia in the late Famennian (late Devonian) in western Laurentia. Palaeogeogr. Palaeoclimatol. Palaeoecol. 589, 110835.
Liu, X.L., 2023. Collision-induced dissociation as "mass spectrometric filter" for rapid screening of tetrapyrrole derivatives and their chelated metal species in complex biological and environmental samples. Rapid Commun. Mass Spectrom. 37, e9413.
Liu, Z., Selby, D., Hackley, P.C., Over, D.J., 2020. Evidence of wildfires and elevated atmospheric oxygen at the Frasnian–Famennian boundary in New York (USA): Implications for the Late Devonian mass extinction: Geological Society of America. Bulletin 132, 2043–2054.
Loboziak, S., Melo, J.H.G., Rodrigues, R., Streel, M., Quadros, L.P., Barrilari, I.M., 1996. Age and correlation of the Barreirinha Formation (Curuá Group, Amazon Basin): new evidence from the miospore biostratigraphy. An. Acad. Bras. Cienc. 68, 207–212.
Lu, M., Ikejiri, T., Lu, Y., 2021. A synthesis of the Devonian wildfire record: Implications for paleogeography, fossil flora, and paleoclimate. Palaeogeogr. Palaeoclimatol. Palaeoecol. 571, 110321.
Lüning, S., Adamson, K., Craig, J., 2003. Frasnian organic-rich shales in North Africa: regional distribution and depositional model. In: Arthur, T., MacGregor, D.S., Cameron, N.R. (Eds.), Petroleum Geology of Africa: New Themes and developing Technologies, 207. Geol. Soc. Lond. Spec. Publ, pp. 165–184.
Lv, Y., Liu, J., Zhu, R., Zhu, J., Chen, Q., Liang, X., He, H., 2022. Photoreductive dissolution of iron (hydr) oxides and its geochemical significance. ACS Earth and Space Chemistry 6, 811–829.
Lyons, T.W., Severmann, S., 2006. A critical look at iron paleoredox proxies: New insights from modern euxinic marine basins. Geochim. Cosmochim. Acta 70, 569–5722.
Mairs, T.M., 1966. A subsurface study of the Fernvale and Viola Formations in the Oklahoma portion of the Arkoma Basin. Tulsa Geol. Soc. Digest 32, 60–81.
Martin, J.H., 1990. Glacial-interglacial CO_2 change: the iron hypothesis. Paleoceanography 5, 1–13.
Martínez-García, A., Sigman, D.M., Ren, H., Anderson, R.F., Straub, M., Hodell, D.A., Jaccard, S.L., Eglinton, T.I., Haug, G.H., 2014. Iron fertilization of the Subantarctic Ocean during the last ice age. Science 343, 1347–1350.
McGhee, G.R., 2013. When the Invasion of Land Failed: The Legacy of the Devonian Extinctions. Columbia University Press, p. 317.
McGlannan, A.J., Bonar, A., Pfeifer, L., Steinig, S., Valdes, P., Adams, S., Duarte, D., Milad, B., Cullen, A., Soreghan, G.S., 2022. An eolian dust origin for clastic fines of Devono-Mississippian mudrocks of the greater north American midcontinent. J. Sediment. Res. 92, 1186–1206.
Milani, E.J., Zalán, P.V., 1999. An outline of the geology and petroleum systems of the Paleozoic interior basins of South America. Episod. J. Int. Geosci. 22, 199–205.
Miller, M.J., Pranter, M.J., Gupta, I., Devegowda, D., Marfurt, C., Sondergeld, C., Rai, C., Mclain, C.T., Packwood, J., Larese, R., 2021. Mississippian Meramec Lithologies and Petrophysical Property Variability, STACK Trend, vol. v. 9. Interpretation, Anadarko Basin, Oklahoma. SE1-SE21.
Mokrosnop, V.M., 2014. Functions of tocopherols in the cells of plants and other photosynthetic organisms: the Ukrainian. Biochem. J. 86, 26–36.
Molinares-Blanco, C.E., 2019. Paleoenvironments and Sediments around the Frasnian/Famennian (F/F) Transition in the Woodford Shale, South Central Oklahoma-a Multiproxy Approach [PhD Dissertation]:. University of Oklahoma, Norman, p. 102.
Montañez, I.P., Poulsen, C.J., 2013. The late Paleozoic ice age: an evolving paradigm. Annu. Rev. Earth Planet. Sci. 41, 629–656.
Nieuwenhuize, J., Maas, Y.E.M., Middelburg, J.J., 1994. Rapid analysis of organic carbon and nitrogen in particulate materials. Mar. Chem. 45, 217–224. https://doi.org/10.1016/0304-4203(94)90005-1.
Northcutt, R.A., Campbell, J.A., 1995. Geological Provinces of Oklahoma: Oklahoma Geological Survey Open-File Report 5–95, 1 Sheet, Scale 1:750000, 6 Page Explanation and Bibliography.
Over, D.J., 1990. Conodont Biostratigraphy of the Woodford Shale (Late Devonian-Early Carboniferous) in the Arbuckle Mountains. south-central Oklahoma [PhD Dissertation]:. Texas Tech University, Lubbock, p. 186.
Over, D.J., 1992. Conodonts and the Devonian-Carboniferous boundary in the Upper Woodford Shale, Arbuckle Mountains, south-central Oklahoma. J. Paleontol. 66, 293–311.
Over, D.J., Barrick, J.E., 1990. The Devonian/Carboniferous boundary in the Woodford Shale, Lawrence uplift, south-Central Oklahoma. In: Ritter, S.M. (Ed.), Early to middle Paleozoic Conodont Biostratigraphy of the Arbuckle Mountains, Southern Oklahoma: Oklahoma Geological Survey, Guidebook, 27, pp. 63–73.
Owens, J.D., Reinhard, C.T., Rohrssen, M., Love, G.D., Lyons, T.W., 2016. Empirical links between trace metal cycling and marine microbial ecology during a large perturbation to Earth's carbon cycle. Earth Planet. Sci. Lett. 449, 407–417.
Parks, D.R., Liu, X.-L., 2023. Distributions of vanadyl and nickel porphyrins in the Woodford Shale and selective chelation of metal species by different tetrapyrrole configurations. Org. Geochem. 186, 104693.
Parrish, J.T., 1982. Upwelling and petroleum source beds, with reference to Paleozoic. Am. Assoc. Pet. Geol. Bull. 66, 750–774.
Perron, M.M., Meyerink, S., Corkill, M., Strzelec, M., Proemse, B.C., Gault-Ringold, M., Rodriguez, E.S., Chase, Z., Bowie, A.R., 2022. Trace elements and nutrients in wildfire plumes to the southeast of Australia. Atmos. Res. 270, 106084.
Perry, W.J., 1989. Tectonic evolution of the Anadarko basin region, Oklahoma. U.S. Geol. Surv. Bull. 1866, 19.
Pew, B.A., 2021. Allogenic Controls on Organic Matter Accumulation in the Woodford Shale in Southern Oklahoma [Masters Thesis]:. Kansas State University, Manhattan, p. 69.
Phillips, R., Xu, J., 2021. A critical review of molybdenum sequestration mechanisms under euxinic conditions: Implications for the precision of molybdenum paleoredox proxies. Earth Sci. Rev. 221, 103799.
Philp, R.P., DeGarmo, C.D., 2020. Geochemical characterization of the Ardmore and Mississippian Woodford Shale from the McAlister Cemetery Quarry, Criner Hills Uplift Ardmore basin, Oklahoma. Mar. Pet. Geol. 112, 104078.
Pohl, C., Fernández-Otero, E., 2012. Iron distribution and speciation in oxic and anoxic waters of the Baltic Sea. Mar. Chem. 145, 1–15.
Poulton, S.W., 2021. The Iron Speciation Paleoredox Proxy, The Iron Speciation Paleoredox Proxy. Cambridge University Press. https://doi.org/10.1017/9781108847148.
Poulton, S.W., Canfield, D.E., 2005. Development of a sequential extraction procedure for iron; implications for iron partitioning in continentally derived particulates. Chem. Geol. 214, 209–221.
Poulton, S.W., Canfield, D.E., 2011. Ferruginous conditions: a dominant feature of the ocean through Earth's history. Elements 7, 107–112.
Poulton, S.W., Raiswell, R., 2005. Chemical and physical characteristics of iron oxides in riverine and glacial meltwater sediments. Chem. Geol. 218, 203–221.
Poulton, S.W., Krom, M.D., Raiswell, R., 2004. A revised scheme for the reactivity of iron (oxyhydr) oxide minerals towards dissolved sulfide. Geochim. Cosmochim. Acta 68, 3703–3715.
Prospero, J.M., Barkley, A.E., Gaston, C.J., Gatineau, A., Campos y Sansano, A., Panechou, K., 2020. Characterizing and quantifying African dust transport and deposition to South America: Implications for the phosphorus budget in the Amazon Basin. Glob. Biogeochem. Cycles 34 p.e2020GB006536.
Rahiminejad, A.H., Zand-Moghadam, H., Mirshahani, M., Khajehzadeh, A., 2022. Famennian inertinite-bearing marine shale facies as indicator of wildfire event in north of Gondwana. Hist. Biol. 34, 1752–1768.
Raiswell, R., Anderson, T.F., 2005. Reactive iron enrichment in sediments deposited beneath euxinic bottom waters: Constraints on supply by shelf recycling. In: McDonald, I., Boyce, A.J., Butler, I.B., Herrington, R.J., Polya, D.A. (Eds.), Mineral Deposits and Earth Evolution, vol. v. 248. Geological Society of London Special Publication, pp. 179–194.
Raiswell, R., Canfield, D.E., 1996. Rates of reaction between silicate iron and dissolved sulfide in Peru margin sediments. Geochim. Cosmochim. Acta 60, 2777–2787.
Raiswell, R., Canfield, D.E., 1998. Sources of iron for pyrite formation in marine sediments. Am. J. Sci. 298, 219–245.
Raiswell, R., Newton, R., Wignall, P.B., 2001. An indicator of water-column anoxia: resolution of biofacies variations in the Kimmeridge Clay (Upper Jurassic, UK). J. Sediment. Res. 71, 286–294.
Raiswell, R., Newton, R., Bottrell, S.H., Coburn, P.M., Briggs, D.E., Bond, D.P., Poulton, S. W., 2008. Turbidite depositional influences on the diagenesis of Beecher's Trilobite Bed and the Hunsrück Slate; sites of soft tissue pyritization. Am. J. Sci. 308, 105–129.
Raiswell, R., Hardisty, D.S., Lyons, T.W., Canfield, D.E., Owens, J.D., Planavsky, N.J., Poulton, S.W., Reinhard, C.T., 2018. The iron paleoredox proxies: a guide to the pitfalls, problems and proper practice. Am. J. Sci. 318, 491–526.
Rickard, D., 2006. The solubility of FeS. Geochim. Cosmochim. Acta 70, 5779–5789.
Rickard, D., Luther, G.W., 2007. Chemistry of iron sulfides. Chem. Rev. 107, 514–562.
Rimmer, S.M., Hawkins, S.J., Scott, A.C., Cressler, W.L., 2015. The rise of fire: fossil charcoal in late Devonian marine shales as an indicator of expanding terrestrial ecosystems, fire, and atmospheric change. Am. J. Sci. 315, 713–733.
Romero, A.M., Philp, R.P., 2012. Organic geochemistry of the Woodford Shale, southeastern Oklahoma: how variable can shales be? Am. Assoc. Pet. Geol. Bull. 96, 493–517.
Rudnick, R.L., Gao, S., 2003. Composition of the Continental Crust. In: Holland, H., Turekian, K. (Eds.), Treatise on Geochemistry, 1st edition. Elsever, Oxford, pp. 1–64.
Sahoo, S.K., Gilleaudeau, G.J., Wilson, K., Hart, B., Barnes, B.D., Faison, T., Bowman, A. R., Larsen, T.E., Kaufman, A.J., 2023. Basin-scale reconstruction of euxinia and late Devonian mass extinctions. Nature 1–6.
Sardar Abadi, M.S., Owens, J.D., Liu, X., Them, T.R., Cui, X., Heavens, N.G., Soreghan, G. S., 2020. Atmospheric dust stimulated marine primary productivity during Earth's penultimate icehouse. Geology 48, 247–251.
Scholz, F., Severmann, S., McManus, J., Hensen, C., 2014. Beyond the Black Sea paradigm: the sedimentary fingerprint of an open-marine iron shuttle. Geochim. Cosmochim. Acta 127, 36–380.

Scholz, F., Schmidt, M., Hensen, C., Eroglu, S., Geilert, S., Gutjahr, M., Liebetrau, V., 2019. Shelf-to-basin iron shuttle in the Guaymas Basin, Gulf of California. Geochim. Cosmochim. Acta 261, 7–92.

Schwartzapfel, J.A., Holdsworth, B.K., 1996. Upper Devonian and Mississippian radiolarian zonation and biostratigraphy of the Woodford, Sycamore, Caney and Goddard formations, Oklahoma. Cushman Foundation for Foraminiferal Research, Special Publication 33, 1–275.

Scotese, C.R., Wright, N., 2018. PALEOMAP Paleodigital Elevation Models (PaleoDEMS) for the Phanerozoic. https://www.earthbyte.org/paleodem-resources-scotese-and-wright-2018/.

Scott, C., Slack, J.F., Kelley, K.D., 2017. The hyper-enrichment of V and Zn in black shales of the late Devonian-early Mississippian Bakken Formation (USA). Chem. Geol. 452, 24–33.

Severmann, S., Lyons, T.W., Anbar, A., McManus, J., Gordon, G., 2008. Modern iron isotope perspective on the benthic iron shuttle and the redox evolution of ancient oceans. Geology 36, 48–490.

Slatt, R.M., Rodriguez, N.D., 2012. Comparative sequence stratigraphy and organic geochemistry of gas shales: commonality or coincidence? J. Nat. Gas Sci. Eng. 8, 68–84.

Slatt, R.M., Galvis-Prtillo, H., Becerra-Rondon, D., Ekwunife, I.C., Brito, R., Zhang, J., Molinares, C., Torres, E., Duarte, D., Milard, B., 2018. Outcrop and subsurface geology applied to drilling, sweet spot and target zone detection of resource shales: the Woodford example. In: Presented at the Unconventional Resource Technology Conference, Houston, Texas USA, 23–25 July. https://doi.org/10.15530/URTEC-2018-2893838. URTEC-2893838-MS.

Song, Y., Gilleaudeau, G.J., Algeo, T.J., Over, D.J., Lyons, T.W., Anbar, A.D., Xie, S., 2021. Biomarker evidence of algal-microbial community changes linked to redox and salinity variation, Upper Devonian Chattanooga Shale (Tennessee, USA). Geol. Soc. Am. Bull. 133, 409–424.

Streel, M., Caputo, M.V., Loboziak, S., Melo, J.H.G., 2000. Late Frasnian–Famennian climates based on palynomorph analyses and the question of the Late Devonian glaciations. Earth Sci. Rev. 52, 121–173.

Sur, S., Owens, J.D., Soreghan, G.S., Lyons, T.W., Raiswell, R., Heavens, N.G., Mahowald, N.M., 2015. Extreme eolian delivery of reactive iron to late Paleozoic icehouse seas. Geology 43, 1099–1102.

Swart, P.K., Oehlert, A.M., Mackenzie, G.J., Eberli, G.P., Reijmer, J.J.G., 2014. The fertilization of the Bahamas by Saharan dust: a trigger for carbonate precipitation? Geology 42, 671–674.

Tang, W., Llort, J., Weis, J., Perron, M.M., Basart, S., Li, Z., Sathyendranath, S., Jackson, T., Sanz Rodriguez, E., Proemse, B.C., Bowie, A.R., 2021. Widespread phytoplankton blooms triggered by 2019–2020 Australian wildfires. Nature 597, 370–375.

Taylor, S.R., McLennan, S.M., 1985. The continental crust: its composition and evolution: an Examination of the Geochemical Record Preserved in Sedimentary Rocks, 1985. Blackwell Scientific Publishing, p. 312.

Tegler, L.A., Sherry, A.M., Herckes, P., Romaniello, S.J., Anbar, A.D., 2023. Up in smoke: Most aerosolized Fe from biomass burning does not derive from foliage. Glob. Biogeochem. Cycles 37 p.e2023GB007796.

Tribovillard, N., Algeo, T.J., Lyons, T., Riboulleau, A., 2006. Trace metals as paleoredox and paleoproductivity proxies: an update. Chem. Geol. 232, 12–32.

Turner, B.W., Slatt, R.M., 2016. Assessing bottom water anoxia within the late Devonian Woodford Shale in the Arkoma Basin, southern Oklahoma. Mar. Pet. Geol. 78, 536–546.

Turner, B.W., Molinares-Blanco, C.E., Slatt, R.M., 2015. Chemostratigraphic, palynostratigraphic, and sequence stratigraphic analysis of the Woodford Shale, Wyche Farm Quarry, Pontotoc County, Oklahoma. Interpretation 3 p.SH1-SH9.

Turner, B.W., Tréanton, J.A., Slatt, R.M., 2016. The use of chemostratigraphy to refine ambiguous sequence stratigraphic correlations in marine mudrocks. An example from the Woodford Shale, Oklahoma, USA. Geol. Soc. London, Journal 173, 854–868.

Ulmisheke, G.F., Klemme, H.D., 1990. Depositional controls, distribution, and effectiveness of world's petroleum source rocks. U.S. Geol. Surv. Bull. 1931, 59.

Wagner, R., Jähn, M., Schepanski, K., 2018. Wildfires as a source of airborne mineral dust–revisiting a conceptual model using large-eddy simulation (LES). Atmos. Chem. Phys. 18, 11863–11884.

Wang, C., Zhai, M., Robbins, L.J., Peng, Z., Zhang, X., Zhang, L., 2024. Late Archean shelf-to-basin iron shuttle contributes to the formation of the world-class Dataigou banded iron formation. Econ. Geol. 119, 725–736.

Weis, J., Chase, Z., Schallenberg, C., Strutton, P.G., Bowie, A.R., Fiddes, S.L., 2024. One-third of Southern Ocean productivity is supported by dust deposition. Nature 629, 603–608.

Wilson, R.D., Schieber, J., Stewart, C.J., 2021. The discovery of widespread agrichnia traces in Devonian black shales of North America: another chapter in the evolving understanding of a "not so anoxic". Ancient sea: PalZ 95, 661–681.

Zhang, J., Slatt, R., 2019. The significance of karst unconformities on overlying resource shales: Lessons learned from the Devonian Woodford Formation applied to the Permian Wolfcamp Shale. Interpretation 7 p.SK33-SK43.

Zhang, F., Dahl, T.W., Lenton, T.M., Luo, G., Shen, S.Z., Algeo, T.J., Planavsky, N., Liu, J., Cui, Y., Qie, W., Romaniello, S.J., 2020. Extensive marine anoxia associated with the late Devonian Hangenberg Crisis. Earth Planet. Sci. Lett. 533, 115976.

Zhang, X., Joachimski, M.M., Gong, Y., 2021. Late Devonian greenhouse-icehouse climate transition: New evidence from conodont δ18O thermometry in the eastern Palaeotethys (Lali section, South China). Chem. Geol. 581, 120383.